

Multistage Localization for High Precision Mobile Manipulation Tasks

Christopher James Mobley

Thesis submitted to the Faculty of the
Virginia Polytechnic Institute and State University
in partial fulfillment of the requirements for the degree of

Masters of Science
in
Mechanical Engineering

Tomonari Furukawa
Brian Lattimer
Kevin Kochersberger

Blacksburg, Virginia

Keywords: Autonomous Navigation, SLAM, Visual Servoing, Mobile Manipulation,
Computer Vision, State Machine
Copyright 2016, Christopher James Mobley

Multistage Localization for High Precision Mobile Manipulation Tasks

Christopher James Mobley

(ABSTRACT)

This paper will show the general framework necessary in order to solve two main problems preventing the development and widespread adoption of automation and robotics in construction (ARC). These problems include the fact that typical construction sites tend to be unstructured and are continuously evolving versus the highly controlled environments found in manufacturing. Also, the relationship between the part and manipulator has been reversed, causing increased complexity not seen in manufacturing environments where the part arrives at a fixed manipulator. The techniques that will be presented allow systems to create a 2-D map of their environment, localize themselves and complete the task(s) assigned. After localizing an augmented reality (AR) tag at the work site, the system is able to use a priori knowledge to localize points of interest (POIs) and complete several different types of operations achieving an accuracy of approximately ± 2 mm based on a multifaceted computer vision approach with only a USB webcam.

Acknowledgments

Insert Acknowledgement

Contents

1	Introduction	1
1.1	Background	1
1.2	Objectives	2
1.3	Summary of Original Contributions	2
1.4	Outline	2
2	Literature Review	3
2.1	Localization and Mapping For Autonomous Mobile Manipulators in Manufacturing and Construction	3
2.2	Task Association and A Priori Knowledge for Mobile Manipulators	3
2.3	Feature Localization Techniques for Mobile Manipulators	3
2.4	Summary	3
3	Fundamentals of Autonomous Robotics	4
3.1	ROS Concepts	4
3.1.1	ROS Communication	5
3.1.2	Rigid Body Transformations	5
3.2	Simultaneous Localization and Mapping Concepts	7
3.3	Localization and Path Planning Concepts	9
3.4	Manipulation Concepts	16
3.5	State Machines Concepts	19
3.6	Camera Concepts	19

3.7	Computer Vision Concepts	23
3.7.1	Color Spaces	23
3.7.2	Linear and Non-Linear Filters	24
3.7.3	Binary Operations	26
3.7.4	Hough Circle Detection	27
3.7.5	Good Feature To Track	29
3.7.6	Optical Flow	32
3.7.7	Pose Estimation and Tracking Through Augmented Reality Tag Detection	34
3.8	Summary	36
4	Multistage Localization for High Precision Mobile Manipulation Tasks	37
4.1	Approach Overview	37
4.2	Global Map Creation and Task Location Specification	38
4.3	Autonomous Localization and Navigation	38
4.4	Task Association and A Priori Knowledge	39
4.5	Generic Framework for Multi-Stage Computer Vision Algorithm	39
4.5.1	Initial Feature Location Prediction	39
4.5.2	Corrected Feature Locations	40
4.6	Approach Implementation	42
4.6.1	System Overview	42
4.6.2	Drilling Framework	43
4.6.3	Sealant Application Framework	44
4.7	Summary	45
5	Experiments and Results	46
5.1	Hardware Architecture	46
5.2	Software Architecture	47
5.3	Experiments	47

5.3.1	Camera Calibration Setup	47
5.3.2	Navigation System Experimental Setup	50
5.3.3	Drilling Operation Experimental Setup	50
5.3.4	Sealant Application Experimental Setup	51
5.4	Results	52
5.4.1	Camera Calibration Accuracy Achieved	52
5.4.2	Navigation System Accuracy Achieved	52
5.4.3	Augmented Reality Tag Accuracy Achieved	57
5.4.4	Drilling Operation Accuracy Achieved	59
5.4.5	Sealant Application Accuracy Achieved	60
5.5	Summary	61
6	Conclusion and Future Work	62
Bibliography		63

List of Figures

1.1	Vision for future transformable production systems.	2
3.1	Simple ROS Node Flowchart. Adapted from [4].	5
3.2	Conversion from Coordinate Frame A to B.	6
3.3	Robot Model with TFs.	6
3.4	Overview of SLAM Framework.	8
3.5	Example of 2-D Occupancy Grid Map Produced.	8
3.6	Real World Performance Analysis of ROS Available SLAM Algorithms. Adapted from [26].	9
3.7	ROS Navigation Stack setup [27].	10
3.8	One-Dimensional Monte Carlo Localization Example. Adapted from [28].	12
3.9	Particle Filter Resampling Example	14
3.10	Visual of AMCL in RVIZ	15
3.11	Trajectory Rollout Path Planning Framework.	16
3.12	Moveit!'s System Architecture.	17
3.13	Forward and Inverse Kinematics Example	18
3.14	Graphical View of State Machine using SMACH	19
3.15	Photometric Image Formation.	20
3.16	Digital Camera Diagram.	21
3.17	Ground Sample Distance Effects on Image Quality.	22
3.18	Shutter Type Effects on Image Quality.	23
3.19	RGB and HSV color space models	24

3.20	Effects of common linear filters.	25
3.21	Histogram equalization depiction.	26
3.22	Effect of histogram equalization on an image.	26
3.23	Effects of common binary operations.	27
3.24	Summary of preprocessing operation performed by Hough Circle detector.	28
3.25	Summary of Hough Circle detector with known radius.	28
3.26	Summary of Hough Circle detector with unknown radius.	29
3.27	Summary of Good Feature detector.	29
3.28	Image Gradient Example.	30
3.29	Difference Between Good Feature and Harris Corner Scoring Functions.	32
3.30	Example of optical flow.	33
3.31	Summary of Kanade-Lucas-Tomasi feature tracker.	34
3.32	Summary of ALVAR AR Tag Detection Framework. Adapted from [37].	36
4.1	Multistage Localization Approach Overview.	37
4.2	2-D map environment with specified start locations.	38
4.3	Robot Localization Framework.	39
4.4	Initial Feature Localization Framework.	39
4.5	Feature Detection and Tracking Pipeline.	41
4.6	Manipulator Correction Control Loop.	42
4.7	General system overview.	43
4.8	Drilling operation framework.	44
4.9	Sealant Application Framework.	45
5.1	Clearpath Robotics' Husky and Fetch Robotics' Fetch Mobile Manipulator	47
5.2	Camera Calibration Setup.	48
5.3	Extracted Corners of Calibration Pattern.	49
5.4	Extracted Corners and Laser Center	49
5.5	Navigation System Experimental Setup.	50

5.6	Drilling Operations Experimental Setup.	51
5.7	Sealant Application Experimental Setup.	52
5.8	Global X and Y Localization Accuracy Given Distance From Start - Clearpath Robotics' Husky.	53
5.9	Global ψ Localization Accuracy Given Distance From Start - Clearpath Robotics' Husky.	54
5.10	Global X and Y Localization Accuracy Given Distance From Start - Fetch Robotics' Fetch.	55
5.11	Global ψ Localization Accuracy Given Distance From Start - Fetch Robotics' Fetch.	56
5.12	Augmented Reality Accuracy Given Specific Start Conditions - Primesense Carmine 1.09.	58
5.13	Augmented Reality Accuracy Given Specific Start Conditions - Microsoft Kinect V2.	59
5.14	Drilling Operation Accuracy Given Distance From Feature Point.	60
5.15	Sealant Application Accuracy Given Distance From Feature Point.	61

List of Tables

3.1	Real World Error Estimation for ROS Available SLAM Algorithm. Adapted from [26].	9
3.2	Comparison Between ROS Available Moveit! Inverse Kinematic Plugins. [Beeson et al. 2015]	18
5.1	Global Localization Accuracy Given Distance From Start - Clearpath Robotics' Husky.	53
5.2	Global Localization Accuracy Given Distance From Start - Fetch Robotics' Fetch.	54
5.3	Augmented Reality Accuracy Given Specific Start Conditions - Primesense Carmine 1.09.	57
5.4	Augmented Reality Accuracy Given Specific Start Conditions - Microsoft Kinect V2.	58
5.5	Drilling Operation Accuracy Given Distance From Work Surface.	59
5.6	Sealant Application Accuracy Given Distance From Work Surface.	60

Chapter 1

Introduction

1.1 Background

Unlike the substantial benefits seen in the manufacturing industry through automation and robotics, automation and robotics in construction (ARC) has lagged far behind in adoption [Balaguer]. Consequently, when compared with other industries, construction has seen a significant decrease in productivity, as well as an increase in workplace injuries/fatalities over the last several decades [Rojas2003]. While several technical complexities inherent in construction have hindered the development and adoption of field construction robots [4], through the capitalization of advances made by other industries, ARC can quickly close this gap. Thereby allowing dangerous and or mundane repetitive tasks to be accomplished autonomously. Thus, causing an increase in productivity and a decrease in workplace injuries/fatalities [1]. However, ARC faces two unique challenges when compared to other industries. Unlike manufacturing environments, which are tightly controlled, typical construction sites tend to lack structure and are continuously evolving. In addition, the reversal in relationship between the part and manipulator has dramatically increased the complexity of the problem to be solved [Feng2015]. Instead of the part appearing at a fixed manipulator, the manipulator must now move to and localize itself with respect to the part. The remainder of this paper is structured as follows: In Section 2, the author's technical approach is outlined, with particular focus on problem two, and experimental results are shown. Conclusions are then drawn and future work discussed in Section 3.

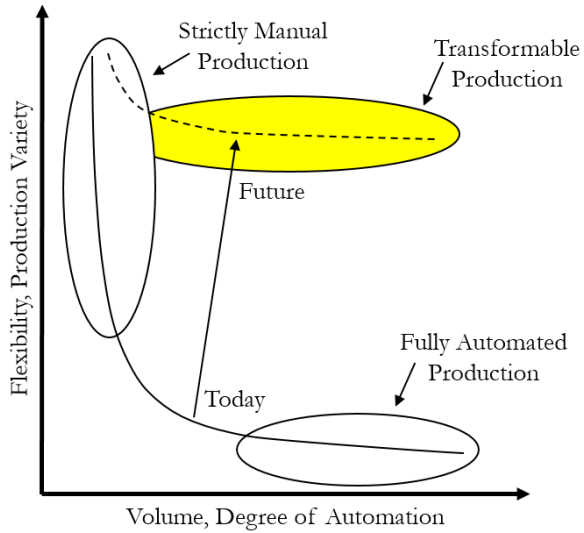


Figure 1.1: Vision for future transformable production systems.

1.2 Objectives

Insert Text Regarding the Objectives of This Work.

1.3 Summary of Original Contributions

Insert Text Regarding the Originals Contributions Presented in this Work.

1.4 Outline

Insert Text Outlining the Upcoming Chapters.

Chapter 2

Literature Review

2.1 Localization and Mapping For Autonomous Mobile Manipulators in Manufacturing and Construction

Insert Text Summarizing Current SLAM and Localization Techniques Used.

2.2 Task Association and A Priori Knowledge for Mobile Manipulators

Insert Text Summarizing Current Methods Used to Associate Mobile Manipulator to a Specific Task and How Prior Knowledge is Conveyed About the Task to be Performed.

2.3 Feature Localization Techniques for Mobile Manipulators

Insert Text Summarizing Current Methods Used to Localize a Feature and Have a Mobile Manipulator Perform a Set Operation.

2.4 Summary

Insert Text Summarizing This Chapter and Transiting to the Next.

Chapter 3

Fundamentals of Autonomous Robotics

The purpose of this chapter is to briefly explain all concepts needed to understand the work presented in the chapters thereafter. The following subsection will explain the basic concepts of the Robot Operating System, Simultaneous Localization and Mapping (SLAM), Localization and Path Planning, as well as Manipulation. In addition, Task Execution using State Machines and the specific Computer Vision Algorithms implemented will be expanded upon.

3.1 ROS Concepts

The Robot Operating System (ROS) [1] is an open-source set of software libraries and tools that aim to simplify the task of creating robotics applications that can be used across a wide variety of platforms. ROS was originally developed in 2007 by Willow Garage as an extension of switchyard, a collection of robotics software developed by Stanford Artificial Intelligence Laboratory in support of the Stanford AI Robot (STAIR) and Personal Robotics (PR) projects. The first distribution of ROS, Box Turtle, was released in 2010. ROS currently has had ten major releases. The most current being Kinetic Kame Turtle, which was released on 23MAY16. In addition ROS boasts tens of thousands of users around the world ranging from hobbyists and researcher to the commercial and industrial industries, as well as hundreds of packages which provide everything from hardware drivers to algorithms for autonomous navigation and manipulation [2]. ROS's large support base act as a force multiplier allows individuals, Labs, or company to concentrate on one particular aspect while capitalizing on work that has already been done.

3.1.1 ROS Communication

ROS uses a name server, called the ROS Master, to maintain a list of nodes and available topics. Nodes communicate with the master server using the XML-RPC protocol. While peer-to-peer communications generally use TCP/IP sockets through the TCPROS protocol. Figure 3.1 shows a simple diagram of two ROS nodes communicating with messages and service topics. In addition to the concepts of messages and services, ROS also employs actions. Actions are similar to service calls, but are designed for long duration tasks that are capable of providing feedback. These communication interfaces provide ROS a great deal of flexibility for robotic applications [3] [4].

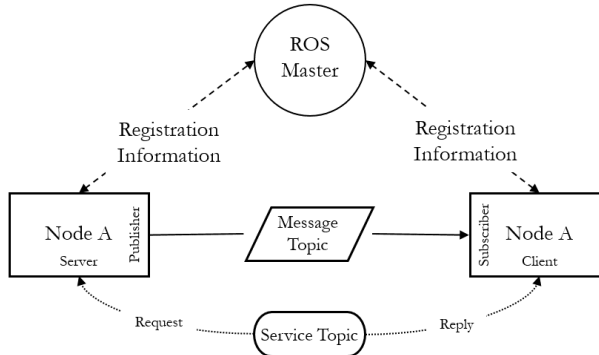


Figure 3.1: Simple ROS Node Flowchart. Adapted from [4].

3.1.2 Rigid Body Transformations

Figure 3.2 shows a purple dot, which represent a point in space. The dot's coordinates in frames a and b are different. A rigid body transform, which can be performed using Equation 3.1, can be used to convert one set of coordinates to another coordinate frame.

$$x_a = T_b^a x_b \quad (3.1)$$

where T_b^a is equal to Equation 3.2

$$\begin{bmatrix} R_b^a & t_b^a \\ 0^T & 1 \end{bmatrix} \quad (3.2)$$

where R_b^a is the rotation matrix, which performs the rotation part of moving frame b into alignment with frame a and t_b^a is the translation matrix, which performs the translation part of moving frame b origin to frame a [5].



Figure 3.2: Conversion from Coordinate Frame A to B.

A robotic system, such as Clearpath Robotics' Husky and Fetch Robotics' Fetch shown in Figure [2](#), typically has many three dimensional coordinate frames that change over time as the robot performs different functions. ROS's TF [6] and TF2 [7] package keep track of coordinate frames and allow for data to be easily converted between these coordinate frames using rigid body transforms. These coordinate frames, as well as robot's links/joints they correspond to, and the rigid transformations between them are set up in the Robot's Unified Robot Description Format (URDF) File [8].

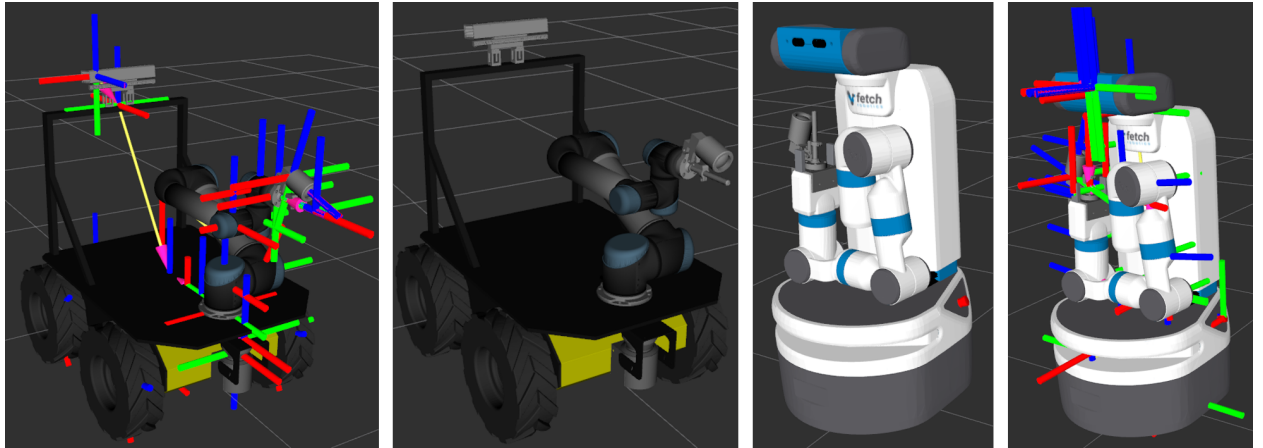


Figure 3.3: Robot Model with TFs.

3.2 Simultaneous Localization and Mapping Concepts

In order for a mobile robot to operate and perform intricate tasks within a complex, GPS-denied environments, such as that of manufacturing facilities, without modifying said environment, the robot must be able to create an accurate map of its environment while simultaneously localizing itself within this map using only on-board sensors. Simultaneous localization and mapping (SLAM) is the problem of building and/or updating a map of an unknown environment while simultaneously localizing the robot within this map [9]. SLAM was pioneered in the early 1990s by Hugh F. Durrant-Whyte and John J. Leonard [10], who based their work on research done by Smith and P. Cheeseman in the mid to late-1980s [11] [12].

Several techniques exist to solve the SLAM problem. Most of these techniques can be categorized into two main paradigms: filtering and optimization-based smoothing [13] [14]. Filtering techniques model the SLAM problem as an incremental state estimation, where the state of the system is composed of the robot's current pose and the map. These estimates are refined at each step by incorporating current sensor measurements. Due to their incremental nature, these SLAM techniques are typically referred to as on-line SLAM approaches. Popular filtering SLAM techniques include the extended kalman filter, particle filter, and information filters. Filtering SLAM techniques have been used widely in past years due to their ability to model different sources of noise and their effect on sensor measurements. However, in recent years optimization-based smoothing techniques have proven to be more efficient, scalable, and robust than that of filtering techniques [14]. Unlike filtering techniques, optimization-based smoothing techniques estimate the robot's entire trajectory and the map. Due to the fact that the final map is based off the robot's entire trajectory and world features instead of the most recent pose and map, these techniques are known as full SLAM approaches. These SLAM techniques incorporate a graph-based structure, where graph nodes represent the robot's pose and world features, while edges represent a spatial constraint relation between two robot poses given by sensor measurements [15]. The graph is optimized using error minimization techniques, such as least-squares, in order to refine the robot's trajectory and map.

In addition to a variety of techniques which can be used to solve the SLAM problem, a wide range of sensors can also be used. Typically sensors include that of a LIDARs, stereo cameras, monocular camera, and RGB-D sensors.

Figure 3.4 shows the generic framework to solving the SLAM problem. In the front-end, raw sensor inputs are processed in order to extract features and perform scan matching; so that, necessary parameters and/or constraints, as well as systems state can be estimated. The systems states and necessary parameters and/or constraints are sent to the back-end of the SLAM algorithm where the systems state is refined and returned based on the parameters and/or constraints.

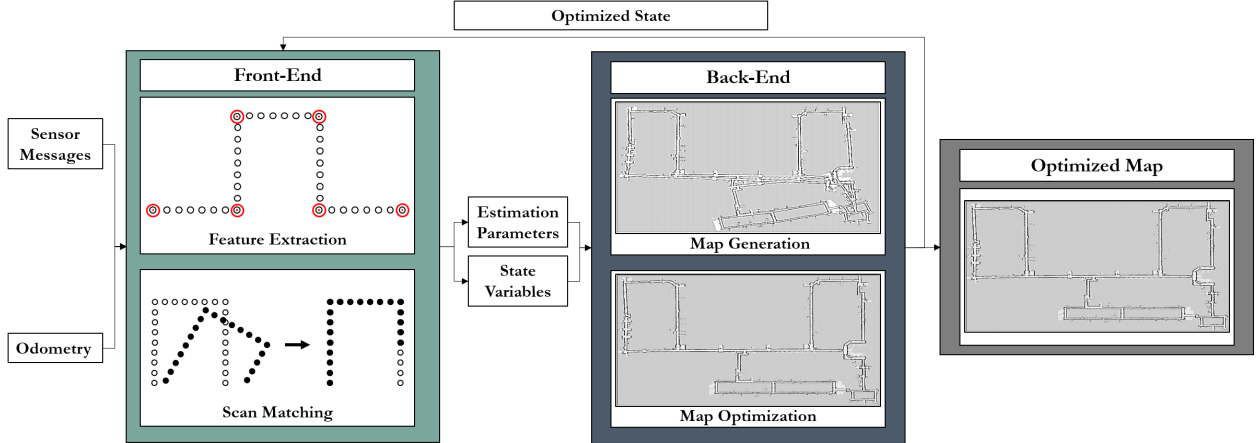


Figure 3.4: Overview of SLAM Framework.

ROS includes several 2-D SLAM packages. These packages are used to build accurate 2-D occupancy grid maps, seen in Figure 3.5. These maps are then used to localize the robot within its environment, as well as to plan and execute appropriate trajectories in order to reach its destination.

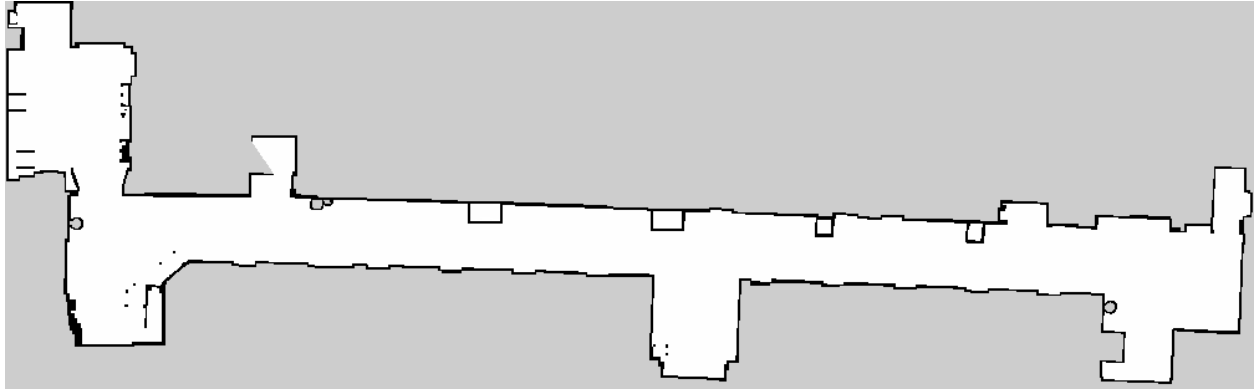


Figure 3.5: Example of 2-D Occupancy Grid Map Produced.

Five of the most common 2-D SLAM ROS packages include HectorSLAM, GMapping, KartoSLAM, CoreSLAM, and LagoSLAM. HectorSLAM [16] is neither a filtering nor an optimization-based smoothing techniques and relies solely on robust scan matching [17]. CoreSLAM [18] and GMapping [19] are filtering SLAM techniques. Both CoreSLAM and GMapping utilize a particle filter. While CoreSLAM employs a very simple particle filter [20], GMapping uses a more complex and efficient Rao-Blackwellized particle filter [21]. Both KartoS LAM [22] and LagoSLAM [23] are optimization-based smoothing SLAM techniques.

However, KartSLAM, which was developed by SRI robotics, uses a highly-optimized and non-iterative Cholesky matrix decomposition for sparse linear systems, known as Sparse Pose Adjustment (SPA) [15] [24], while LagoSLAM uses LAGO optimizer developed by Carlone et al [25].

Figure 3.6 and Table 3.1 show the aforementioned 2-D SLAM ROS packages real world performance based on testing done by Santos et al [26]. KartSLAM achieved the smallest error demonstrating the robustness of its sparse pose adjustment (SPA) and that of full SLAM techniques in general. As a result, KartSLAM was used to generate Figure 2 as well as the maps used during testing of the multistage localization approach presented in this paper.

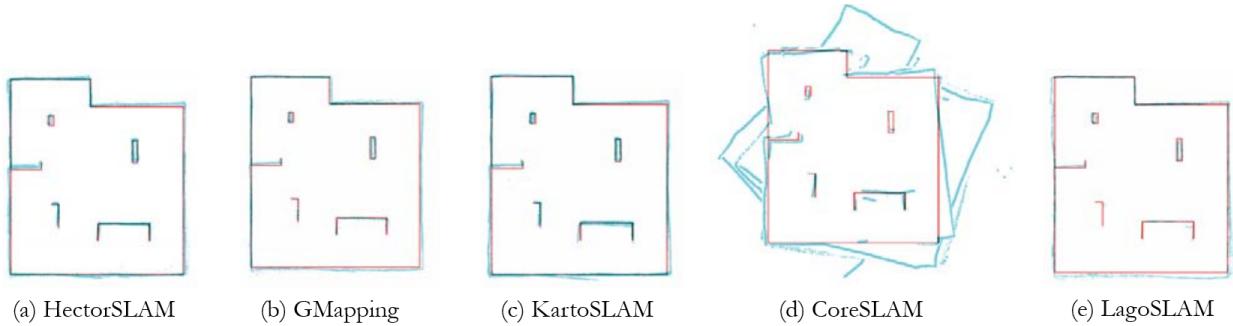


Figure 3.6: Real World Performance Analysis of ROS Available SLAM Algorithms. Adapted from [26].

Table 3.1: Real World Error Estimation for ROS Available SLAM Algorithm. Adapted from [26].

Real World Experiments				
HectorSLAM	GMapping	KartoSLAM	CoreSLAM	LagoSLAM
1.1972	2.1716	1.0318	14.75333	3.0264
0.5094	0.6945	0.3742	7.9463	0.8181
1.0656	1.6354	0.9080	7.5824	2.5236

3.3 Localization and Path Planning Concepts

ROS's Navigation Stack is a collection of packages, which uses odometry and laser scan data, as well as a goal position and orientation in order to output the velocity commands

needed to reach the specified goal. Figure 3.7 shows an overview of how the individual packages work together to achieve this objective. The Map_Server node loads a previously generated two-dimensional grid map. Once the AMCL node receives the map, odometry, and laser scan data, it is able to localize the robot within the provided map, using the Adaptive Monte Carlo Localization technique for which it gets its name. The Move_Base node maintains both global and local planners and costmaps. Information about obstacles in the world are stored in these costmap. The global costmap is used for long-term planning, while the local costmap is used for short-term planning and obstacle avoidance. The global planner computes an optimal path to the goal given the starting state of robot and the global costmap. While the local planner computes shorter trajectories given the current state of the robot and the local costmap. Once a path is developed, Move_Base outputs the necessary velocity commands needed in order to reach the specified destination [27].

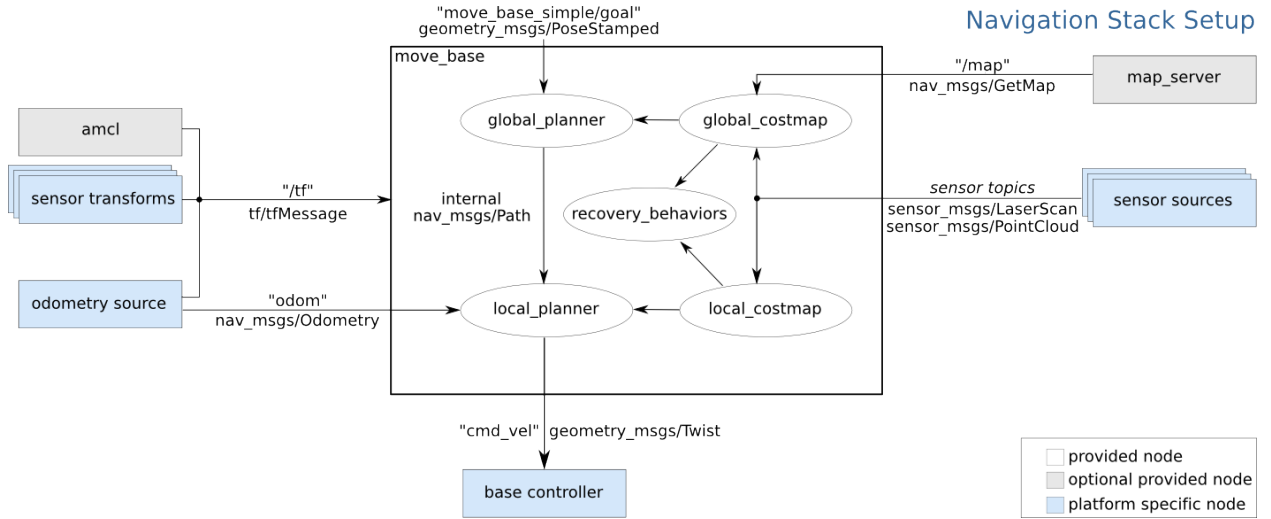


Figure 3.7: ROS Navigation Stack setup [27].

After building a two-dimensional occupancy grid map, shown in Figure 3.5, using SLAM, it becomes crucial to accurately localize the robot within this predefined map; so that, the robot can both plan and execute appropriate trajectories to reach its destination. Localization involves estimating the position and orientation of the robot, known collectively as pose, while the robot moves throughout its environment. One routine localization technique used involves tracking the robot from an initial known starting pose. Through the measurement of wheel rotation and the integration of accelerations provided by an inertial measurement unit (IMU), the distance traveled by the robot from the initial position can be calculated and the robot's pose in the map estimated with some certainty. However, these methods do not account for wheel slippage or measurement error. As a result, the accuracy of the pose estimate will degrade over time. Consequently, a solution which can compensate for the accumulated odometry error and inaccuracies in the initial starting pose is needed.

One accepted solution to this problem is Monte Carlo Localization (MCL), which utilizes a particle filters to keep track of the robot's pose. However, additional options include Kalman Filters and Markov Localization, which employ Gaussian distributions and histograms respectively.

Figure 3.8 depicts MCL using a one-dimensional corridor with a few doors. The robot initially has no information about where it is in this corridor. As a result, the graph of the robot's belief states, which defines the probability of the robot being at a particular position, is drawn from a uniform distribution of discretely sampled positions along the corridor. A measurement update is performed at each time step. A measurement update involves convolving the measurement model, the probability of receiving a specific sensor measurement in the corridor, with the belief states to get an updated belief state. The updated belief state is the same as the previous belief state; however, the weight of each particle have been updated based on the sensor reading. At step k=1 the robot senses a door; so, the weight of particles at the three door are increased. At the next step, a motion model update is performed. The odometry indicated that the robot moved forward a specified distance d. As a result, the belief state is updated by moving the particles forward that specific distance with noise added to account for the aforementioned odometry errors. It should be noted that the particles at this stage in Figure 3.8 were also resampled, which will be covered in the following paragraphs. The motion model update is followed by a measurement update. The robot again senses a door. As a result, the measurement model is the same as the previous time step. After convolving the current measurement model with the current belief state, the cumulative probability mass is centered at door two indicating that the robot is likely at this location [28].

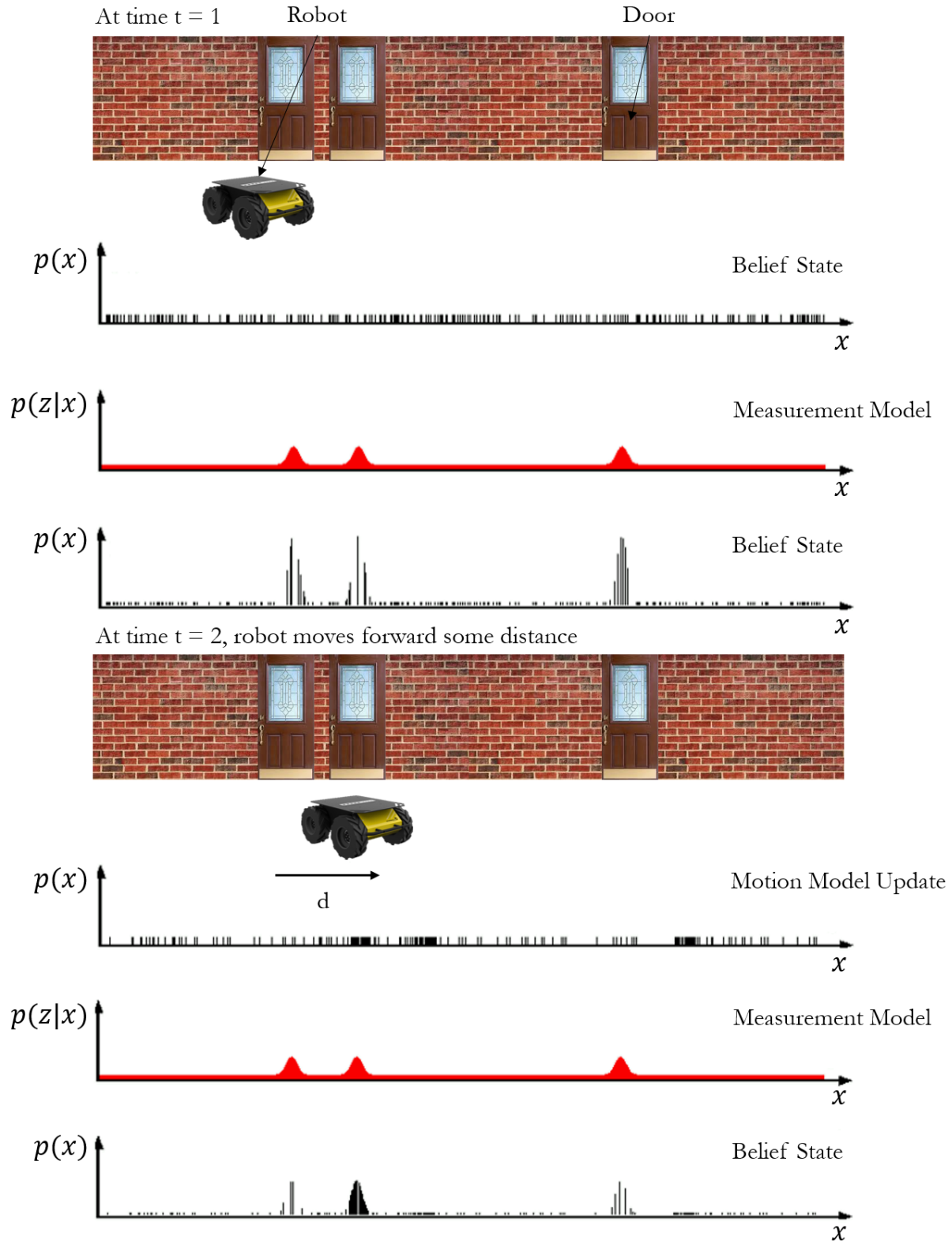


Figure 3.8: One-Dimensional Monte Carlo Localization Example. Adapted from [28].

Two-dimensional MCL follows the same format of a motion model and then measurement update. The initial particles are drawn from the current odometry with added noise. At each step, the particles are updated via the odometry and then corrected via a measurement update. For each particle, the correlation between the two-dimensional occupancy grid map, seen in Figure 3.5, and laser scan is calculated using Equation 3.3, where A is the predefined map, B is the map created by the current laser scan, and \bar{A} and \bar{B} are the mean values of the pixels of both maps respectively. Note that while obstacle pixels are black and have a value of 1, free space pixels are grey and have a value of 0. While m and n are the x and y values of the pixel. The particle (pose) with the highest correlations score is chosen as the pose for the current step. The weight of each particles at step k is found by multiplying the particles weight at step $k - 1$ by its normalized correlation score at time step k , as seen in Equation 3.4.

$$s = \frac{\sum_m \sum_n (A_{mn} - \bar{A})(B_{mn} - \bar{B})}{\sqrt{(\sum_m \sum_n (A_{mn} - \bar{A})^2)(\sum_m \sum_n (B_{mn} - \bar{B})^2)}} \quad (3.3)$$

$$W_k \leftarrow W_{k-1}s \quad (3.4)$$

As weights are multiplied over steps, the particles with consecutive small correlation scores are reduced to very small values. As a result, the particles filter eventually has every few effective particles to ensure that good results are produced. Consequently, re-sampling, show in Figure 3.9, is performed when the number of effective particles become too small. This is done by drawing samples close to the particles that have a higher weights, indicated by their size. Thus the new sample have a higher density near the position where the particle with higher weight existed. Each particle after resampling has same weight. As a result, the particle filter begins from scratch.

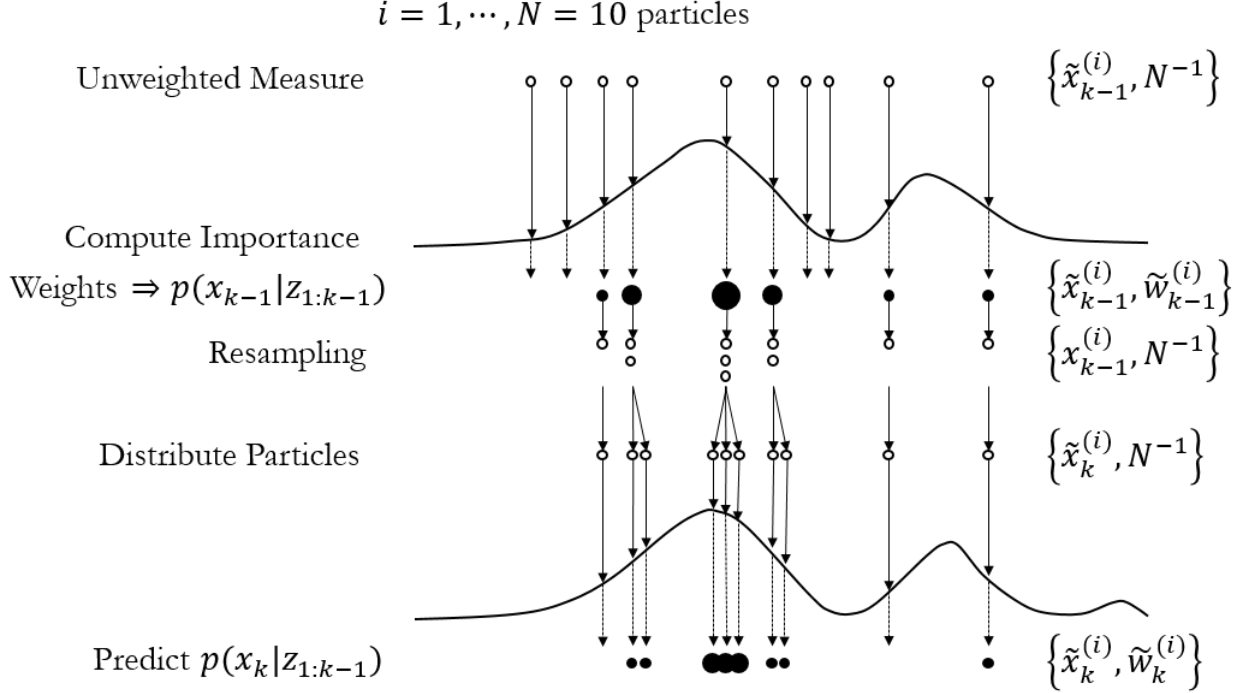


Figure 3.9: Particle Filter Resampling Example

Due to the computational complexity inherent in iteratively having to calculate the correlation score for each particle, an optimization technique known as *KLD-sampling* is used. *KLD-sampling*, derived from *Kullback-Leibler divergence*, is a technique that determine the number of particles needed such that the error between the sample and true posterior is less than ϵ [28]. KLD-sampling basically control the number of particles based on the difference in odometry and particle base location.

Figure 3.10 shows how KLD-sampling effectively work. Initially when the position is unknown, the particle cloud is large due to the uncertainty in the position and orientation of the robot. However, as the robot moves, the particle converges and the particle cloud size reduces as KLD-sampling removes the redundant particles and improves computational performance.

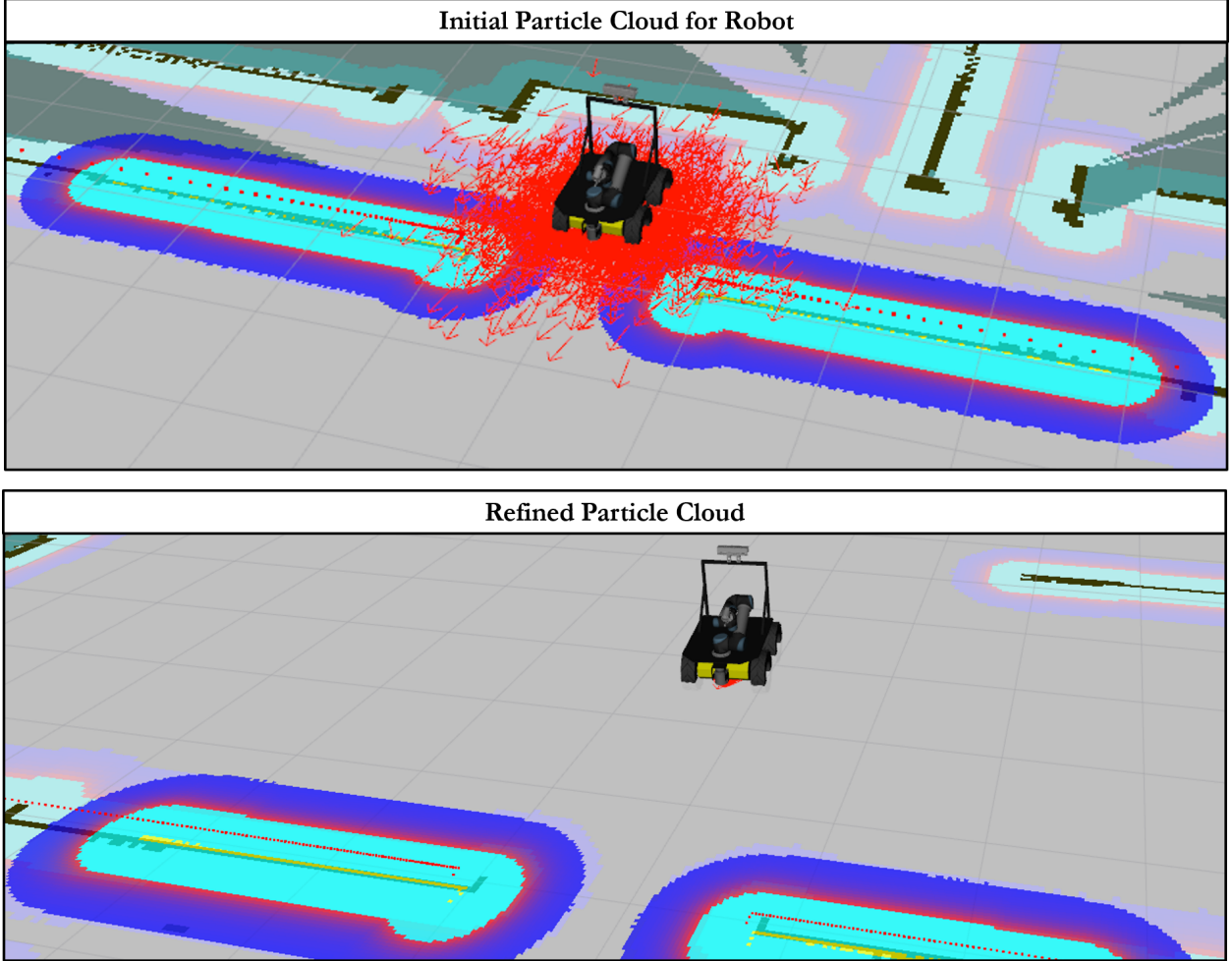


Figure 3.10: Visual of AMCL in RVIZ

After calculating the local and global costmaps, as well as the location of the robot within the given map, the robot must now both plan and execute appropriate trajectories to its destination. Two frequent techniques used are the Dynamic Window Approach (DWA) and Trajectory Rollout. Both sample the space of feasible controls. For a differential drive robot, such as Clearpath Robotics' Husky and Fetch Robotics' Fetch, this controls space is 2D and consists of translations and rotational velocities, $\dot{x}, \dot{\theta}$, which are limited by the robot's capabilities. Each sampled velocity is forward simulated from the robot's current for a short period of time in order to generate simulated trajectories as shown in Figure 3.11. These simulated trajectories are then scored using the cost function in Equation 3.5.

$$C(k) = \alpha Obs + \beta Gdist + \gamma Pdist + \delta \frac{1}{\dot{x}^2} \quad (3.5)$$

Where Obs is the sum of grid cell cost through which the trajectory passes (taking account of the robot's actual footprint in the grid); $Gdist$ and $Pdist$ are the estimated shortest distance from the endpoint of the trajectory to the goal and the optimal path, respectively; and \dot{x} is the translation component of the velocity command that produces the trajectory.

The simulated trajectory that minimizes this cost function is chosen. As a result, chosen trajectories tend to keep obstacles at a distance, proceed towards the goal, remain near the optimal path, as well as have higher velocities [29]. DWA and Trajectory Rollout differ in that Trajectory Rollout samples achievable velocities over the entire forward simulation, while DWA sample only from achievable velocities for just one simulation step [30].

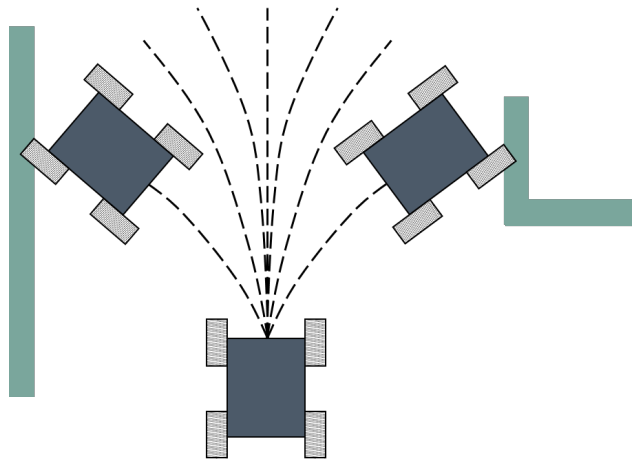


Figure 3.11: Trajectory Rollout Path Planning Framework.

3.4 Manipulation Concepts

Insert Text Outlining Moveit!'s System Architecture.

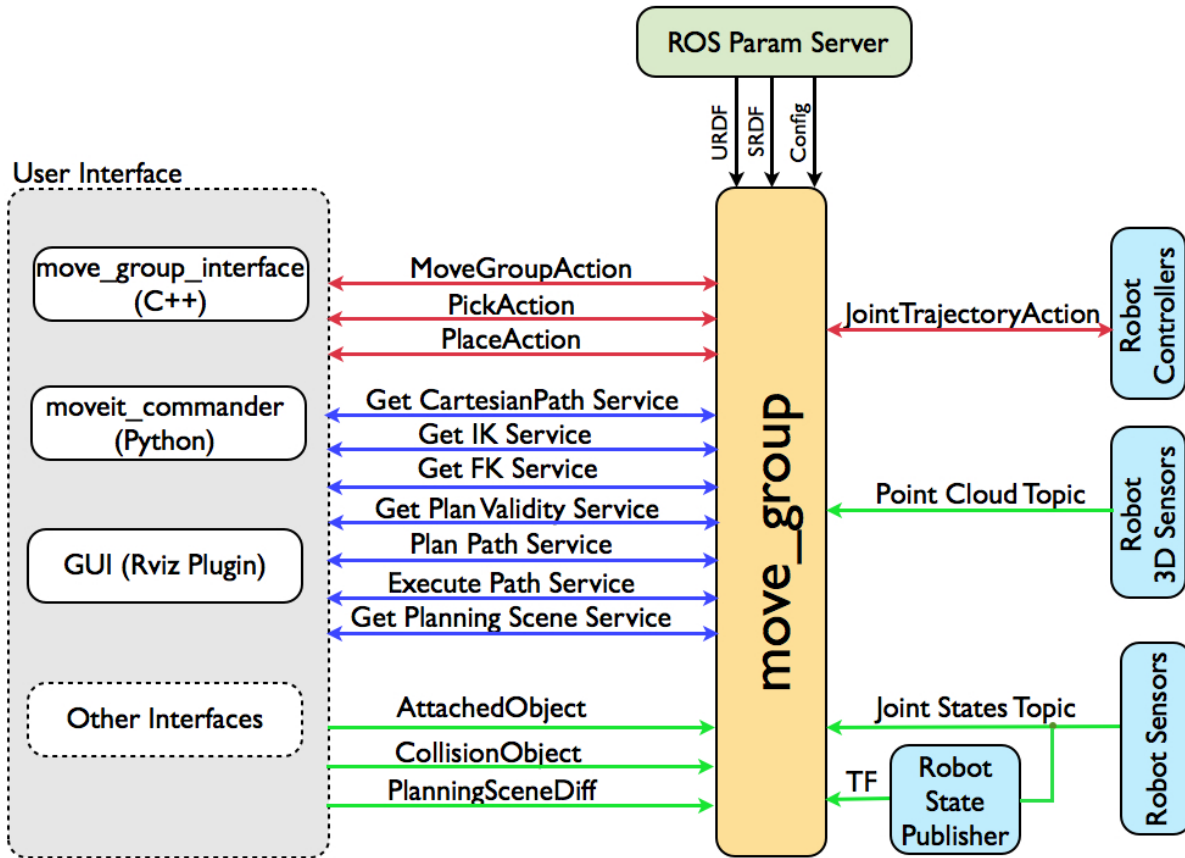


Figure 3.12: Moveit!'s System Architecture.

Insert Text Explaining the Basic Intuition Behind Forward and Inverse Kinematics.

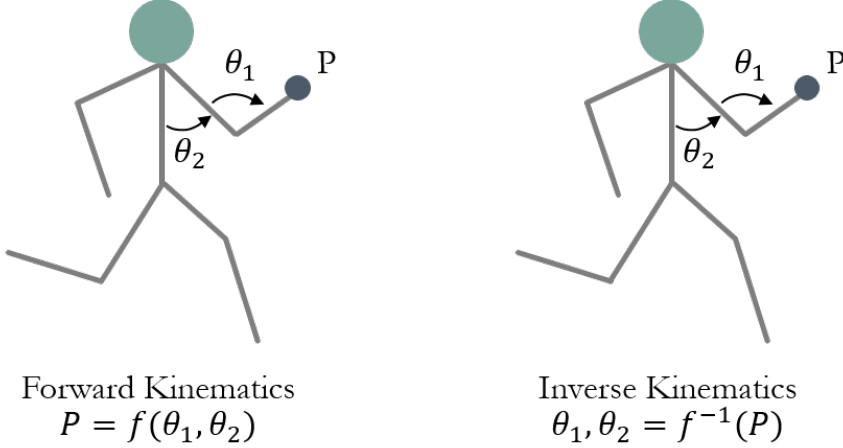


Figure 3.13: Forward and Inverse Kinematics Example

Insert Test Explaining the Difference Between The Numerical Solvers available in ROS (KDL, KDL-RR and Trac_IK) and Why Trac_IK was chosen to be used.

Table 3.2: Comparison Between ROS Available Moveit! Inverse Kinematic Plugins. [Beeson et al. 2015]

Robot	DOFs	IK Technique					
		Orcos' KDL		KDL-RR		TRAC-IK	
		Solve Rate (%)	Avg Time (ms)	Solve Rate (%)	Avg Time (ms)	Solve Rate (%)	Avg Time (ms)
Atlas 2013 Arm	6	75.54	1.35	97.13	0.39	99.97	0.33
Atlas 2015 Arm	7	75.71	1.50	93.13	0.81	99.18	0.48
Baxter Arm	7	61.07	2.21	89.52	1.02	99.17	0.60
Denso VS-068	6	27.92	3.69	98.13	0.42	99.78	0.38
Fanuc M-430iA/2F	5	21.07	3.99	88.34	0.92	99.16	0.58
Fetch Arm	7	92.49	0.73	93.82	0.72	99.96	0.44
Jaco2	6	26.23	3.79	97.66	0.58	99.51	0.58
LBR iiWA 14 R820	7	37.71	3.37	94.02	0.73	99.63	0.56
KUKA LWR 4+	7	67.80	1.88	95.40	0.62	99.95	0.38
PR2 Arm	7	83.14	1.37	86.96	1.27	99.84	0.59
NASA Robonaut2 'Grasping Leg'	7	61.27	2.29	87.57	1.10	99.31	0.67
NASA Robonaut2 'Leg + Waist + Arm'	15	97.99	0.80	98.00	0.84	99.86	0.79
NASA Robonaut2 Arm	7	86.28	1.02	94.26	0.73	99.25	0.50
NASA Robosimian Arm	7	61.74	2.44	99.87	0.36	99.93	0.44
TRACLabs Modular Arm	7	79.11	1.35	95.12	0.63	99.80	0.53
UR10	6	36.16	3.29	88.05	0.82	99.47	0.49
UR5	6	35.88	3.30	88.69	0.78	99.55	0.42
NASA Valkyrie Arm	7	45.18	3.01	90.05	1.29	99.63	0.61

3.5 State Machines Concepts

Insert Text Explaining the Basics of State Machine and How They are Implemented in SMACH.

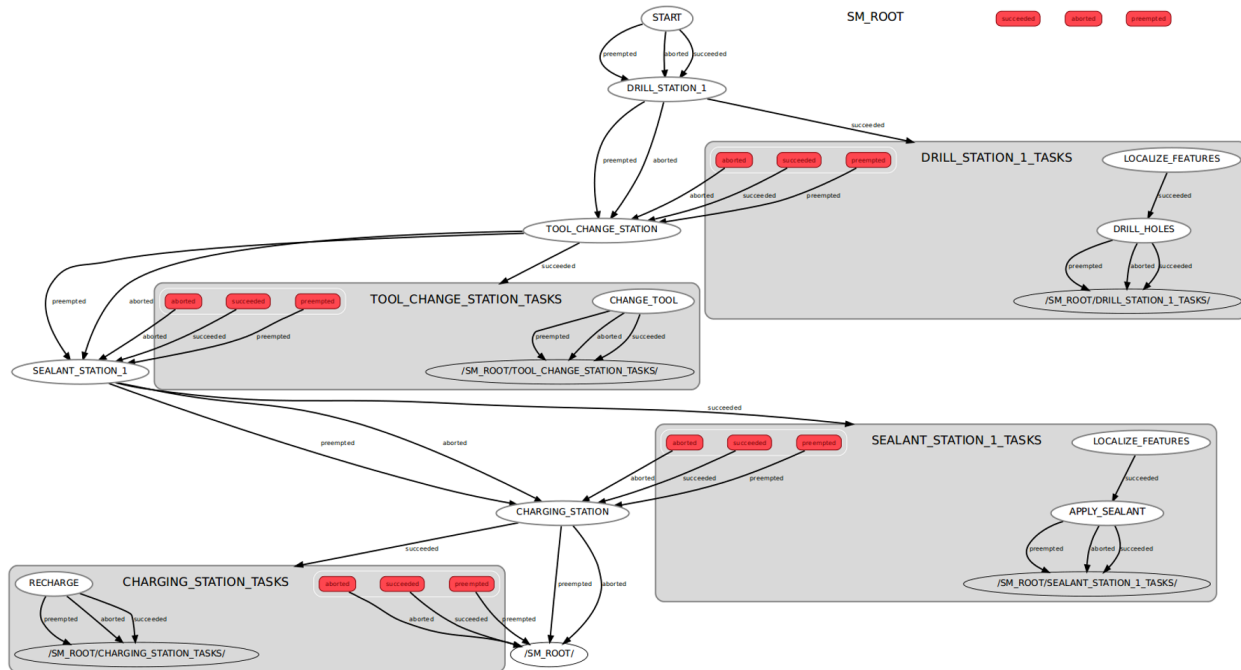


Figure 3.14: Graphical View of State Machine using SMACH

3.6 Camera Concepts

Insert Text Explaining How Digital Image Are Formed and Stored.

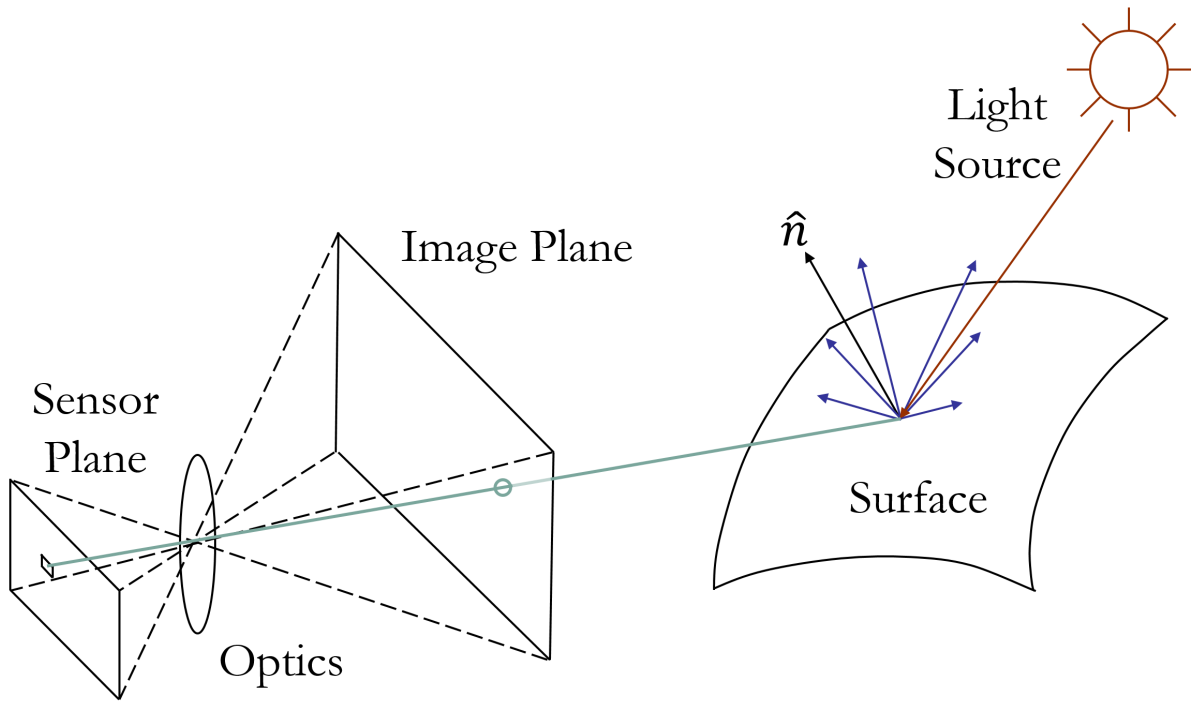


Figure 3.15: Photometric Image Formation.

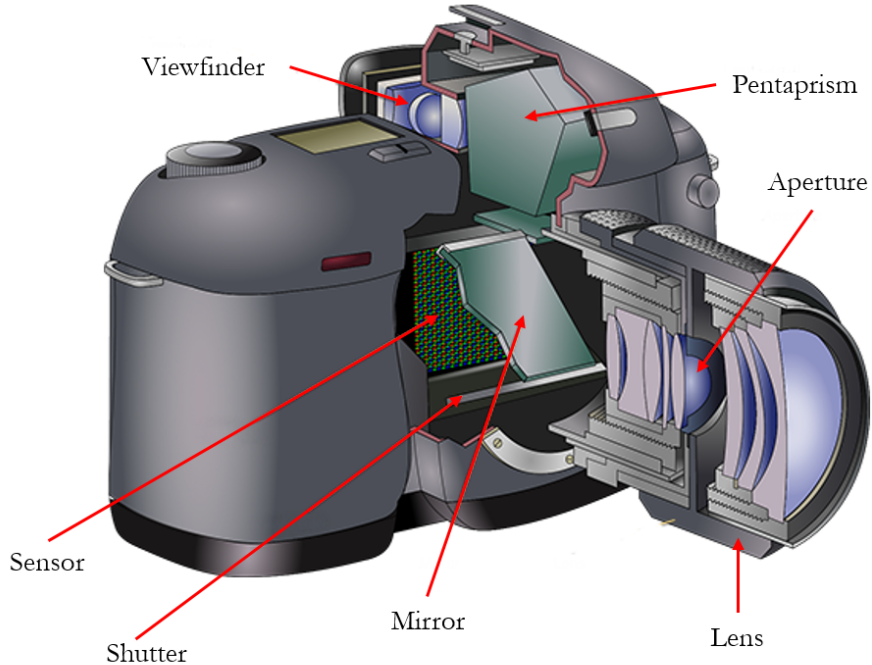


Figure 3.16: Digital Camera Diagram.

Insert Text Explaining Ground Sample Distance and It's Effects on Image Quality Thereby Effecting Ones Camera Choice.

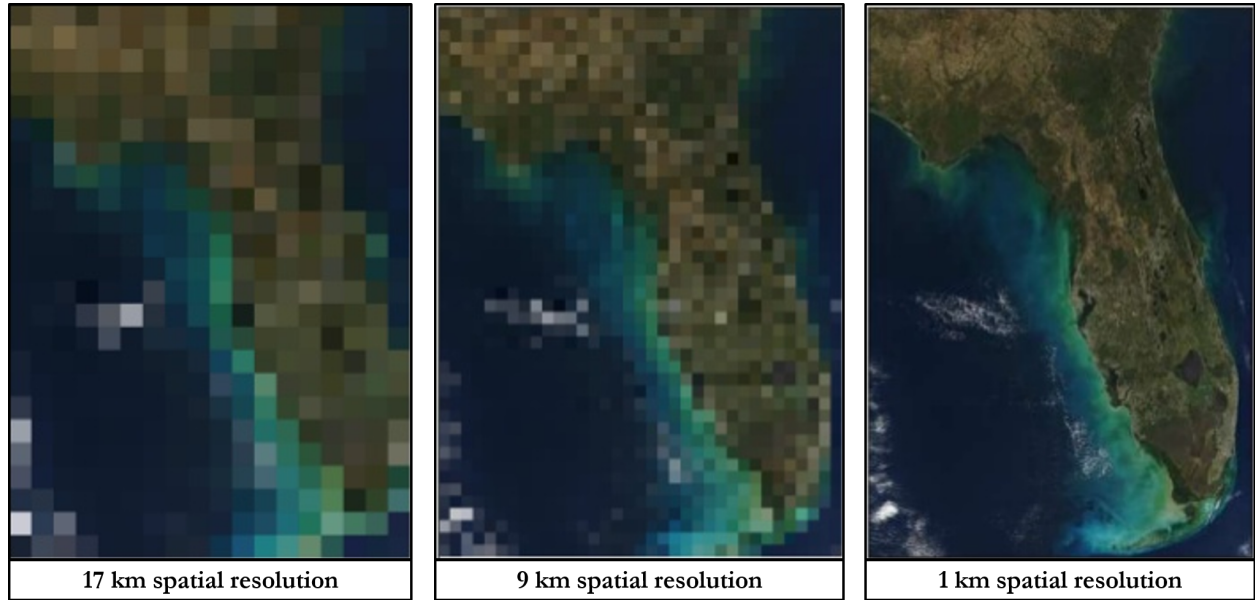


Figure 3.17: Ground Sample Distance Effects on Image Quality.

Insert Text Explaining The Effects of Different Shutter Type on Image Quality Thereby Effecting Ones Camera Choice.

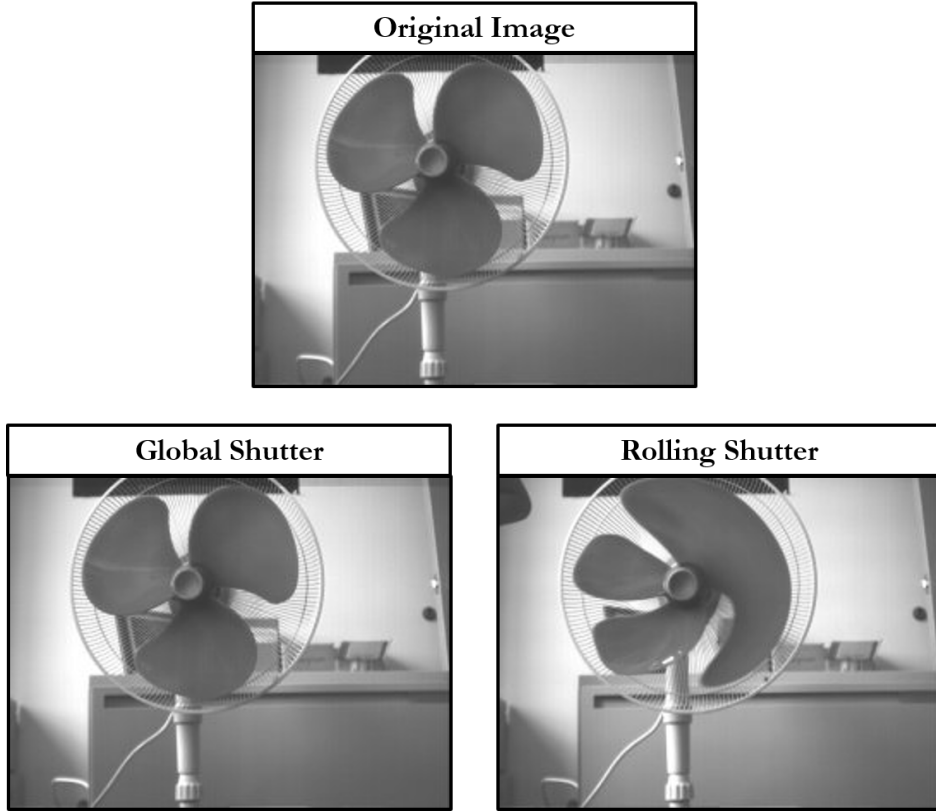


Figure 3.18: Shutter Type Effects on Image Quality.

3.7 Computer Vision Concepts

Insert Text Regarding Upcoming Sections.

3.7.1 Color Spaces

While the RGB color space is the primary color space used to describe spectral content of color signals, a variety of other representations have been developed [31]. Each color space has unique advantages and disadvantages that must be considered before using a specific color space for a given application. The two color spaces used in the multistage localization approach presented in this paper are the RGB and the HSV color spaces, depicted in Figure 3.19. The RGB color space is an additive color space based on the RGB color model, in which red, green, and blue light is added together to produce any color that is the triangle defined by those three primary colors [32], [33]. The HSV color space, which was developed by Alvy Ray Smith in 1978, is a cylindrical-coordinate representations of points in the RGB color model [34]. In some situations, such as color picking, the HSV model is more intuitive,

as it mirrors traditional color mixing methods [35]. HSV stands for hue, saturation, and value. Hue represents angular position on the color wheel, where red starts at 0° , green at 120° , and blue at 240° . Saturation, or distance from the center axis, indicates the amount of grey in a color, where 0 is the color grey and 1 is the primary color. Value, or distance along the center axis, represent the brightness of a color, where 0 is black and 1 is white [34].

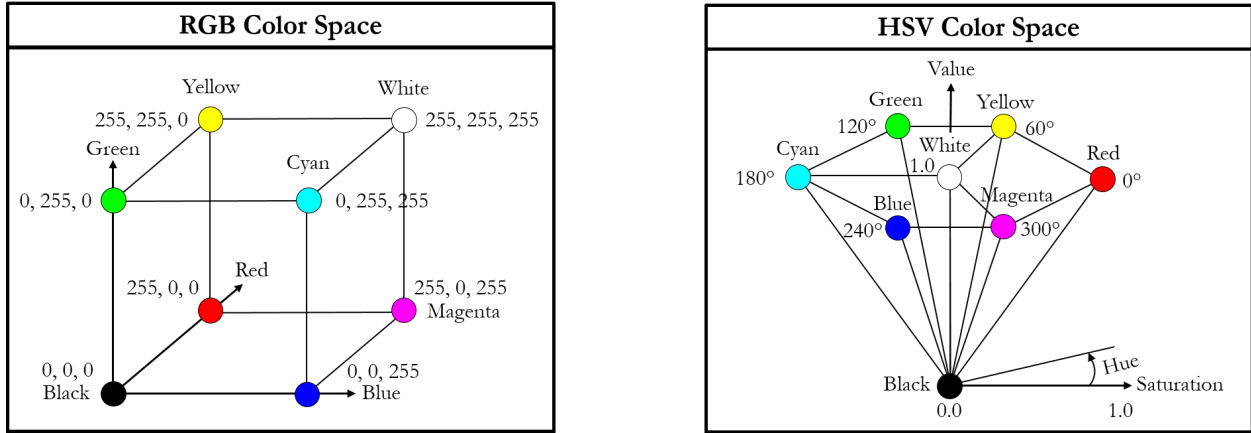


Figure 3.19: RGB and HSV color space models

3.7.2 Linear and Non-Linear Filters

Insert Text Explaining the Basics behind Linear Filters, Which Ones Were Chosen and Why.

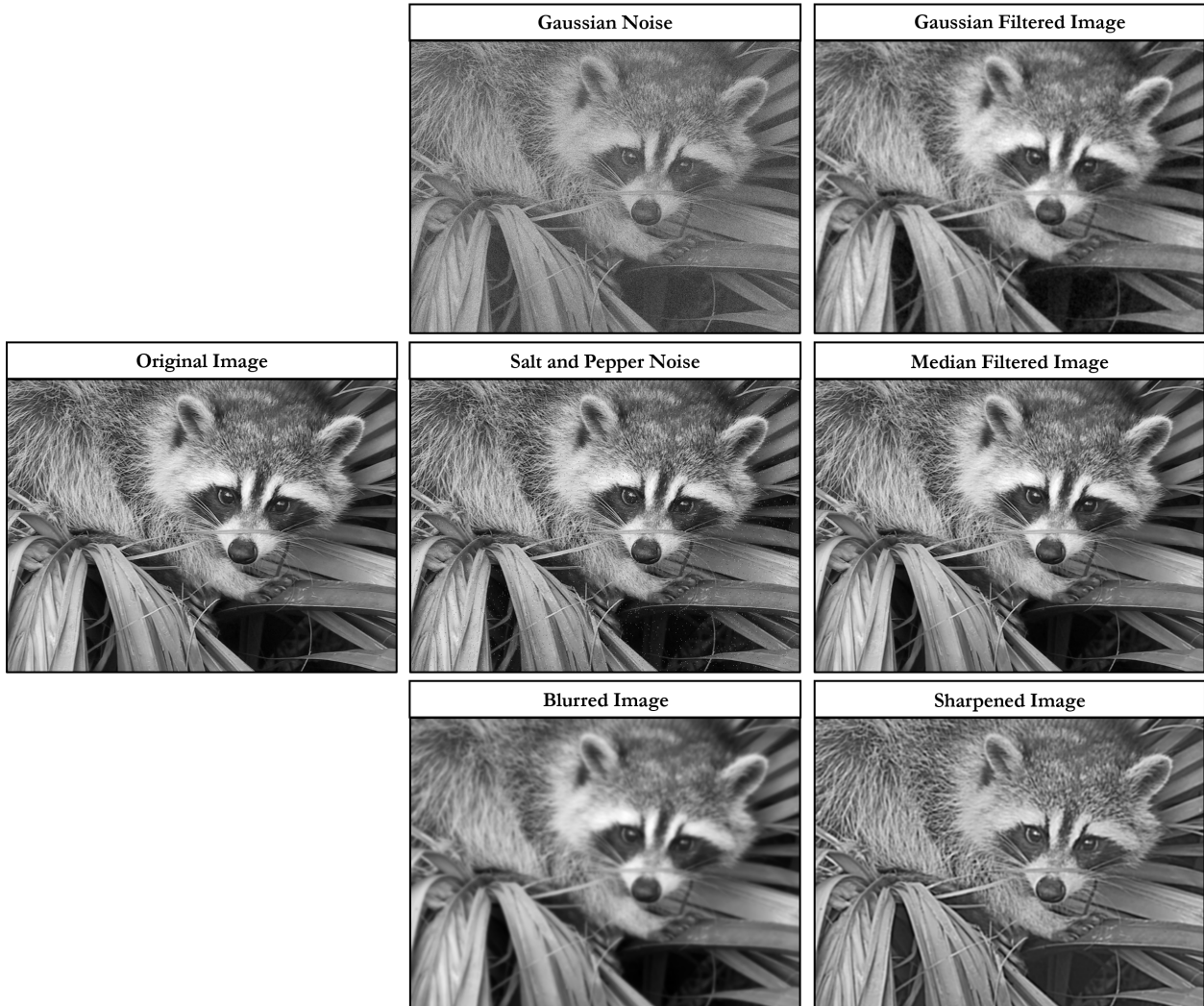


Figure 3.20: Effects of common linear filters.

Insert Text Explaining the Basics behind Histogram Equalization.

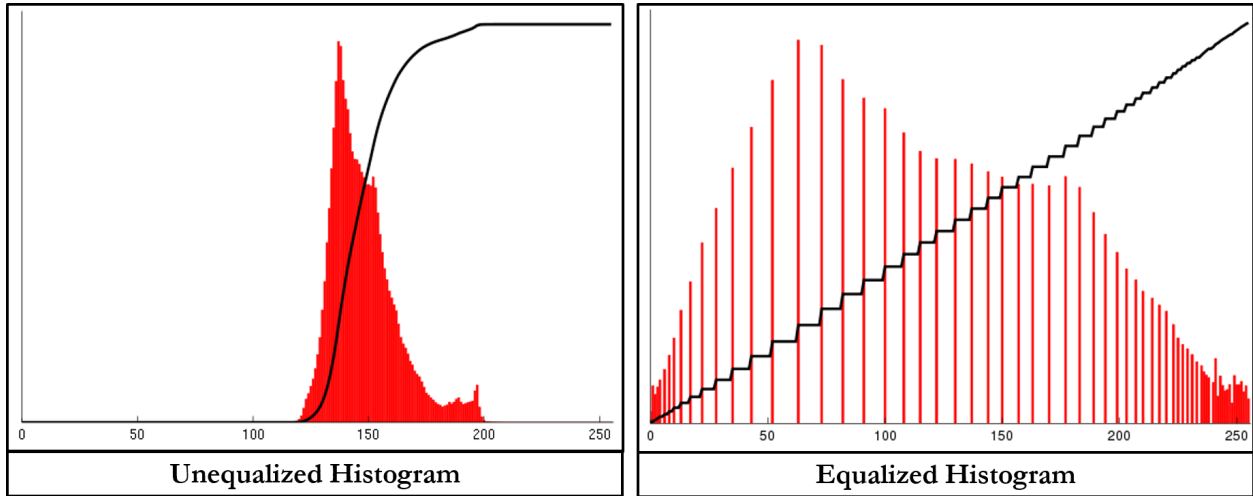


Figure 3.21: Histogram equalization depiction.

Insert Text Explaining The Effect of Histogram Equalization on Images.



Figure 3.22: Effect of histogram equalization on an image.

3.7.3 Binary Operations

Insert Text Explaining the Basics behind Binary Operations, Which Ones Were Chosen and Why.

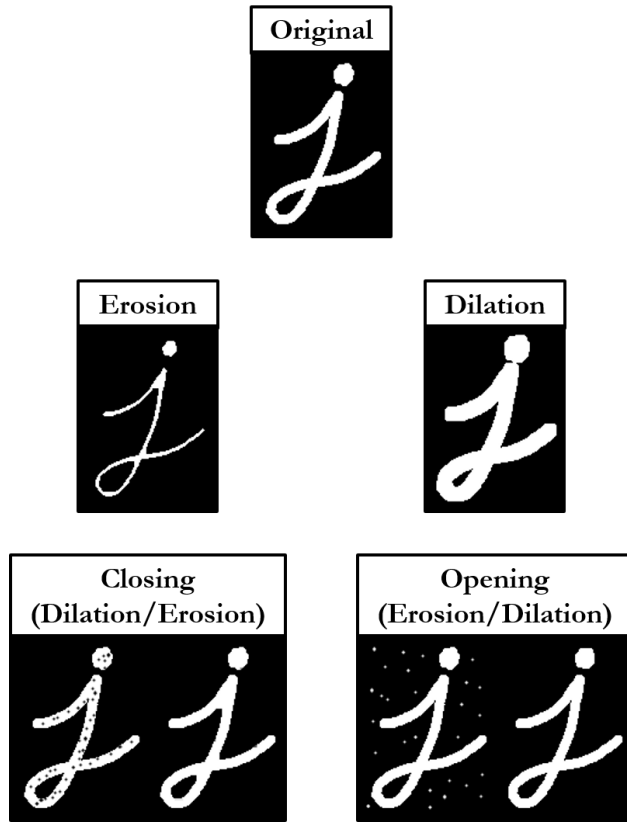


Figure 3.23: Effects of common binary operations.

3.7.4 Hough Circle Detection

Insert Text Explaining The Basic Preprocessing Operation Performed by Hough Circle Transform In Order to Get Edges.

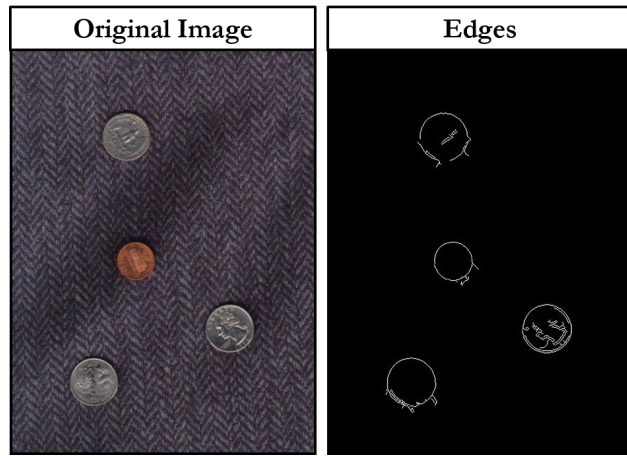


Figure 3.24: Summary of preprocessing operation performed by Hough Circle detector.

Insert Text Explaining the Basic Intuition Behind Hough Circle with Known Radius.

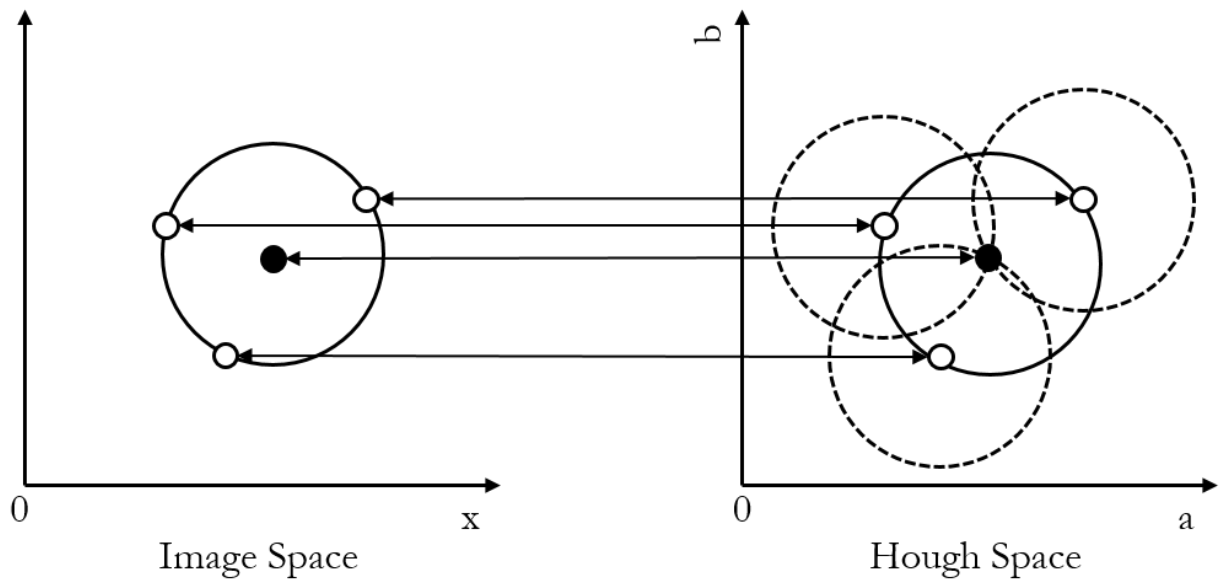


Figure 3.25: Summary of Hough Circle detector with known radius.

Insert Text Expanding Basic Intuition Behind Hough Circle with Unknown Radius.

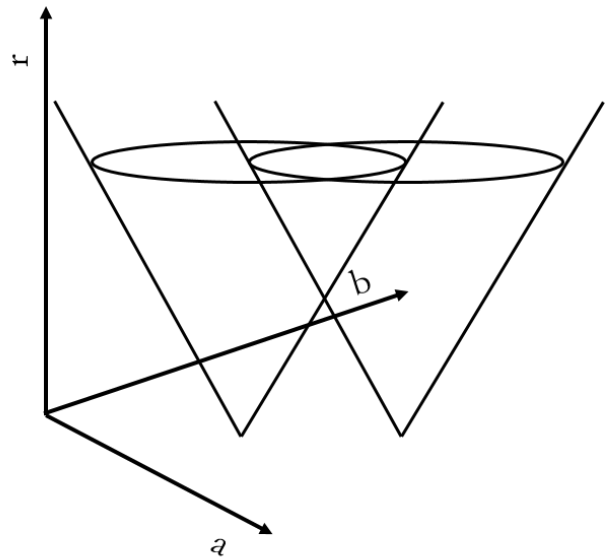


Figure 3.26: Summary of Hough Circle detector with unknown radius.

3.7.5 Good Feature To Track

Insert Text Explaining the Basic Intuition Behind Good Feature.

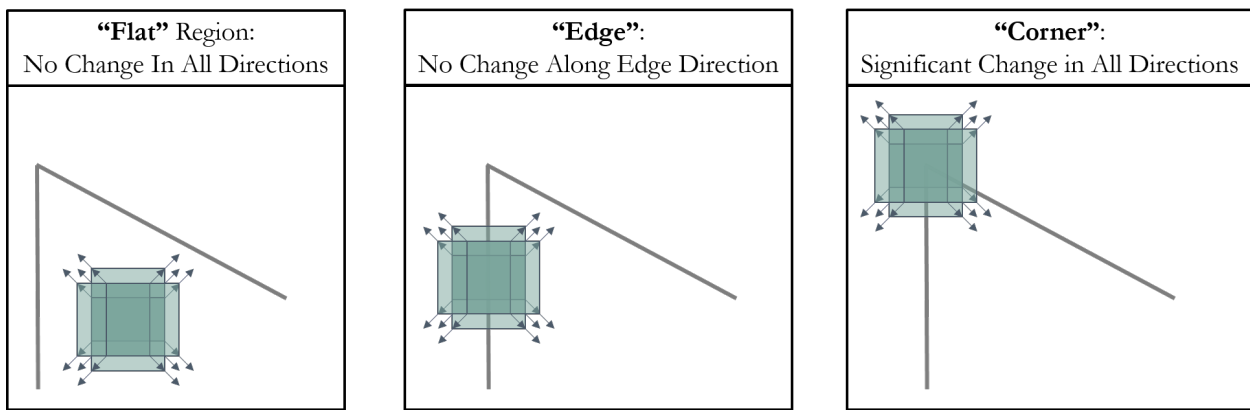


Figure 3.27: Summary of Good Feature detector.

Insert Text Explaining an Image Gradient/Derivative and Why We Look for Them.

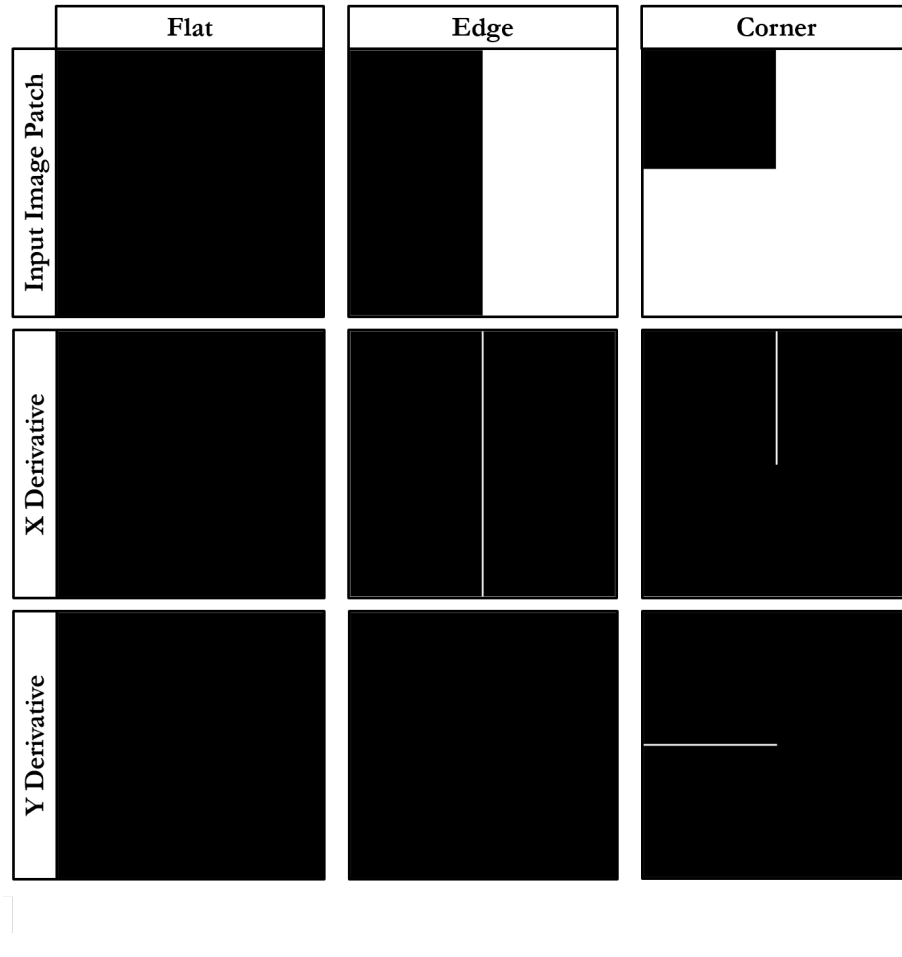


Figure 3.28: Image Gradient Example.

Insert Text Explaining Math.

$$E(u, v) = \sum_{x,y} w(x, y)[I(x + u, y + v) - I(x, y)]^2 \quad (3.6)$$

$$\sum_{x,y} [I(x + u, y + v) - I(x, y)]^2 \quad (3.7)$$

$$E(u, v) \approx \sum_{x,y} [I(x, y) + uI_x + vI_y - I(x, y)]^2 \quad (3.8)$$

$$E(u, v) \approx \sum_{x,y} u^2 I_x^2 + 2uv I_x I_y + v^2 I_y^2 \quad (3.9)$$

$$E(u, v) \approx [u \ v] \left(\sum_{x,y} w(x, y) \begin{bmatrix} I_x^2 & I_x I_y \\ I_x I_y & I_y^2 \end{bmatrix} \right) \begin{bmatrix} u \\ v \end{bmatrix} \quad (3.10)$$

$$E(u, v) \cong [u \ v] M \begin{bmatrix} u \\ v \end{bmatrix} \quad (3.11)$$

Where

$$M = \sum_{x,y} w(x, y) \begin{bmatrix} I_x^2 & I_x I_y \\ I_x I_y & I_y^2 \end{bmatrix}$$

Insert Text Explaining How Both Harris Corner and Good Feature Scoring Functions Work and Why Good Feature Performs Slightly Higher.

$$R = \det(M) - k(\text{trace}(M))^2 \quad (3.12)$$

Where $\det(M) = \lambda_1 \lambda_2$ and $\text{trace}(M) = \lambda_1 + \lambda_2$. So,

$$R = \lambda_1 \lambda_2 - k(\lambda_1 + \lambda_2)^2 \quad (3.13)$$

$$R = \min(\lambda_1, \lambda_2) \quad (3.14)$$

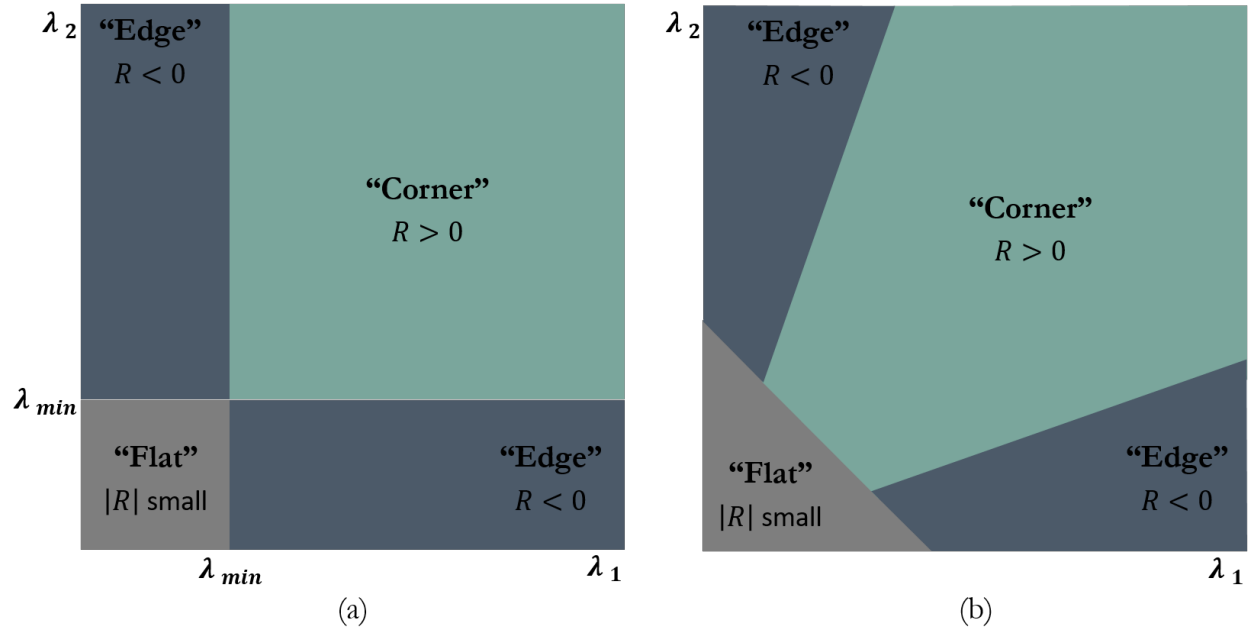


Figure 3.29: Difference Between Good Feature and Harris Corner Scoring Functions.

3.7.6 Optical Flow

Insert Text Explaining the Basic Intuition Behind Optical Flow.



Figure 3.30: Example of optical flow.

Insert Text Explaining the Basic Intuition Behind Kanade-Lucas-Tomasi Feature Tracker.

$$\sum_x [T(\mathbf{W}(\mathbf{x}; \Delta \mathbf{p})) - I(\mathbf{W}(\mathbf{x}; \mathbf{p}))]^2 \quad (3.15)$$

$$\sum_x \left[T(\mathbf{W}(\mathbf{x}; \mathbf{0})) + \nabla T \frac{\partial \mathbf{W}}{\partial \mathbf{p}} \Delta \mathbf{p} - I(\mathbf{W}(\mathbf{x}; \mathbf{p})) \right]^2 \quad (3.16)$$

$$\Delta \mathbf{p} = H^{-1} \sum_x \left[\nabla T \frac{\partial \mathbf{W}}{\partial \mathbf{p}} \right]^T [I(\mathbf{W}(\mathbf{x}; \mathbf{p})) - T(\mathbf{x})] \quad (3.17)$$

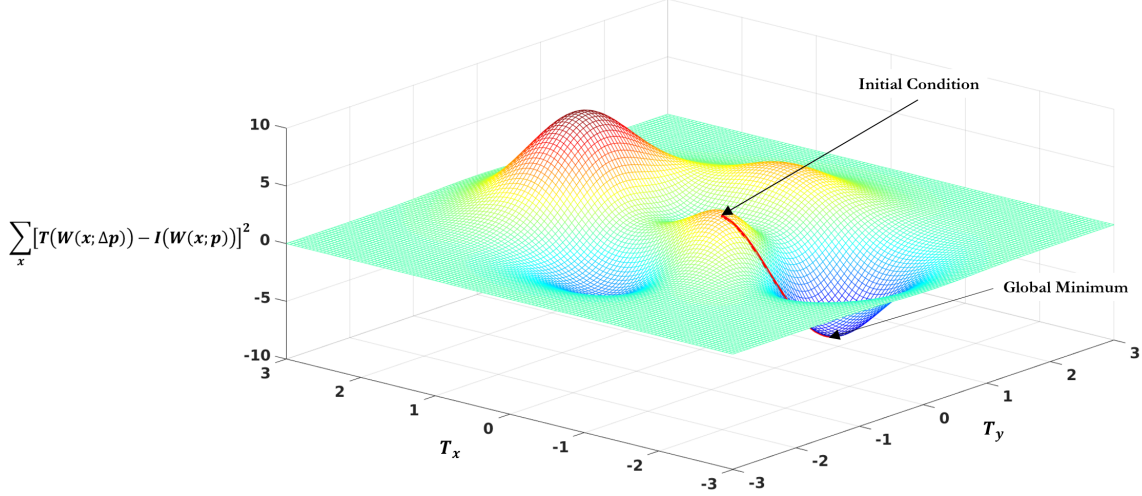


Figure 3.31: Summary of Kanade-Lucas-Tomasi feature tracker.

3.7.7 Pose Estimation and Tracking Through Augmented Reality Tag Detection

AR tags, which are also known as fiducial markers, are artificial landmarks which are designed to be easy to detect and identify under most circumstances [36]. Consequently, the detection method must be robust to changes in luminance (brightness), chrominance (color), and resolution, as well as be scale and rotationally invariant. Once detected and identified, AR tags can be used to accurately calculate the pose (location and orientation) of a camera, as well as to encode information or associate it with each tag's specific identity [37]. Using AR tag to calculate the relative pose of a camera in real-time is called marker-based tracking. Several straightforward and robust marker-based tracking toolkits exist, such as ARToolKit [38], ALVAR [39], and AprilTags [36]. The multistage localization approach presented in this paper will use a ROS implementation of ALVAR [40] to both calculate the pose of an AR tag in the camera's frame and associate information with that tag's specific identity.

Figure 3.32 shows ALVAR's marker-based tracking framework. The system first acquires a greyscale image, either directly or through conversion from another image format. After which, adaptive thresholding, which can handle local changes in luminance, is used to create a binary image. A binary image consists of a background, black pixels, and objects, sections of white pixels. Subsequently, the contours of each object are found. Due to the fact that AR systems, like ALVAR, aim for real-time processing and fast performance, time cannot be wasted processing non-markers. As a result, fast acceptance/rejection tests are run. ALVAR uses two fast accept/reject tests including size and the four-corner test. The number of pixels

in an object's perimeter can be efficiently used to estimate the object's area. Objects with areas that are either too large or too small can be rejected. Even if an object, whose area is too small, is a marker, it is too far from the camera to either be correctly identified or the pose of the camera accurately calculated. Objects, whose area is too large, can be rejected given some background knowledge about the upper and lower range of the camera from the marker, as well as the marker's size. The contours of all remaining markers are fitted with lines. A quadrilateral has exactly four straight lines and four corners. The number of lines and corners of each object are calculated. Those that fail the four-corner test are dropped. After determining that an object is a marker, it is identified and the corner locations are optimized to sub-pixel accuracy for further calculations. Even small errors in the detected 2-D locations of edges and corners can significantly affect the calculated pose of the camera [37]. The pose of a calibrated camera can be uniquely determined from a minimum of four coplanar but non-collinear points [41]. Thus, the system can calculate a marker's pose (relative to camera) in 3-D coordinates using the four corner points of the marker in image coordinates.

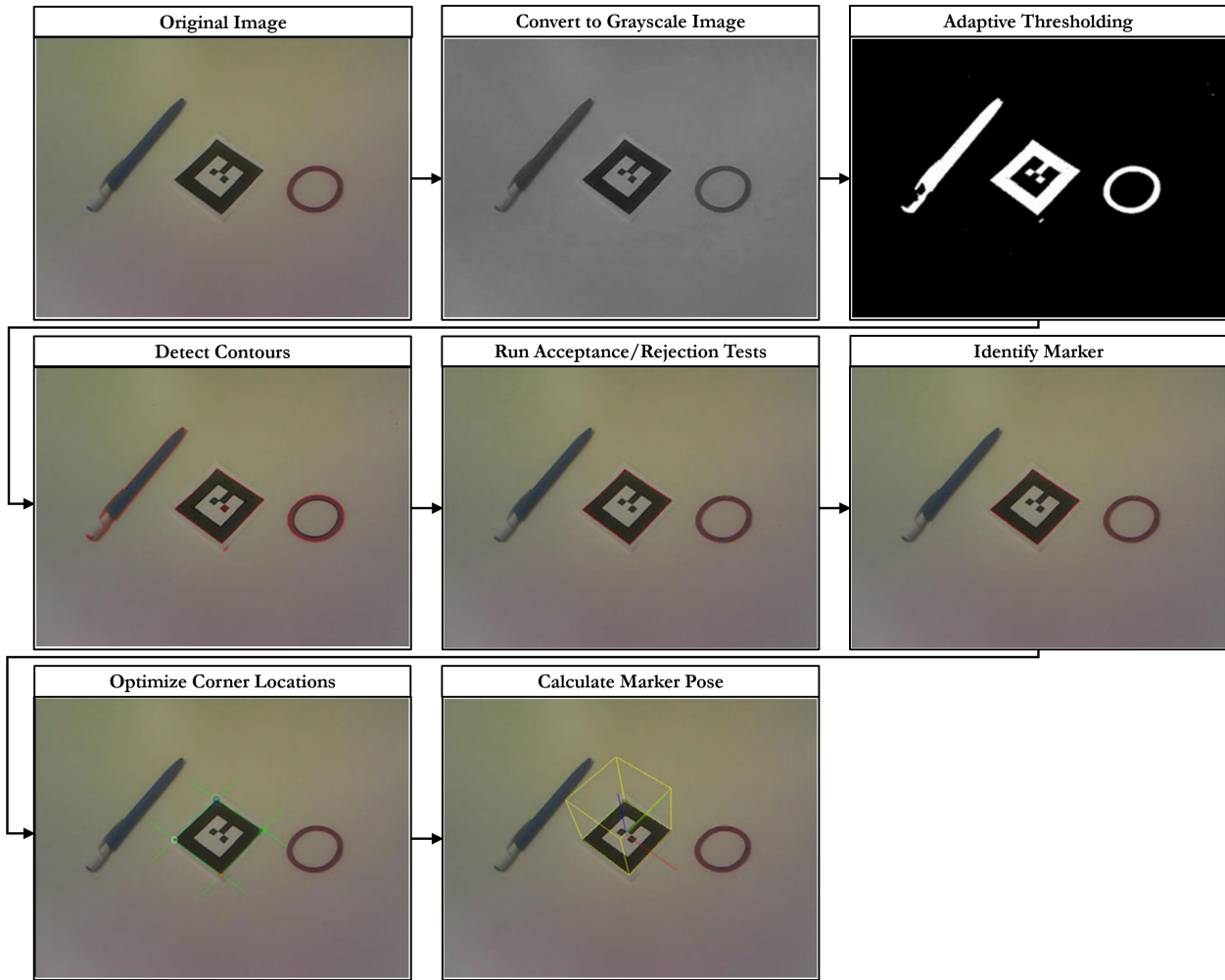


Figure 3.32: Summary of ALVAR AR Tag Detection Framework. Adapted from [37].

3.8 Summary

Insert Text Summarizing This Chapter and Transiting to the Next.

Chapter 4

Multistage Localization for High Precision Mobile Manipulation Tasks

Insert Text Outlining the Upcoming Sections.

4.1 Approach Overview

Insert Text Outlining the Steps of the Approach.

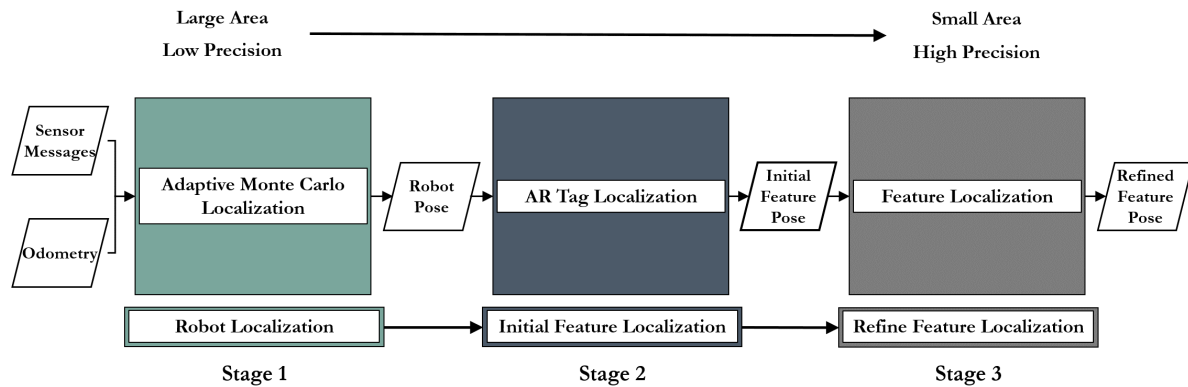


Figure 4.1: Multistage Localization Approach Overview.

4.2 Global Map Creation and Task Location Specification

The purpose of this section is reiterate why KartoSLAM was chosen, as well as describe how maps are created, the map files themselves, and how global locations are specified.

Before the manipulator can localize itself with respect to the part, the system must first navigate to the general vicinity in which the work will take place. In order to achieve this, the system utilizes odometry data, given by wheel encoders and an onboard inertial measurement unit (IMU), as well as sensor data, such as laser scans from a LIDAR or point clouds from an RGB-D sensor, to output safe velocity commands that will be sent to the mobile base of the system.

First, a Simultaneous Localization and Mapping (SLAM) technique named KartoSLAM uses the system's odometry and laser scan or point cloud data, to create a 2-D map of the environment in which the operation(s) will take place. After which, the global location of specific operation(s) are defined, as shown in Figure 4.2.

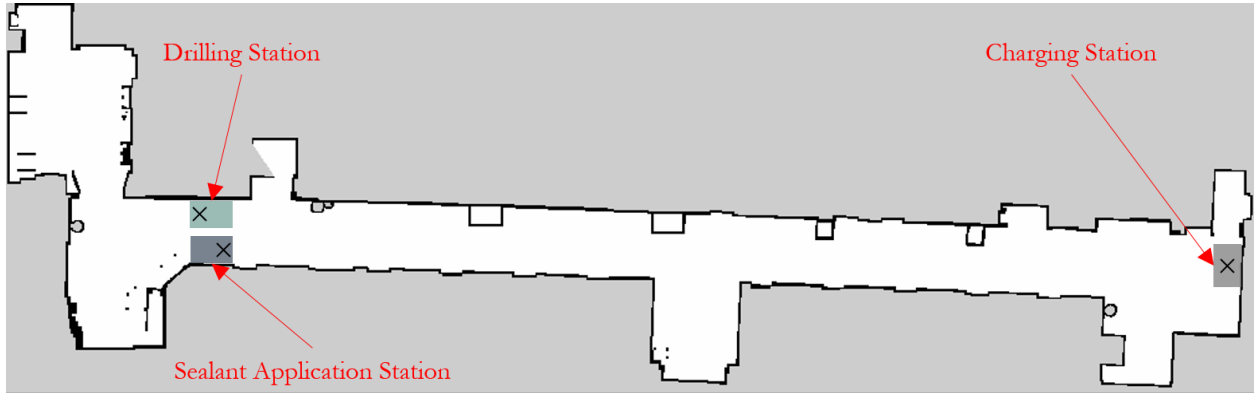


Figure 4.2: 2-D map environment with specified start locations.

4.3 Autonomous Localization and Navigation

Adaptive Monte Carlo localization (amcl) is used to localize the system within the map. Subsequently, odometry data is combined with a global and local cost map, in which obstacles and a specific distance around them represent a cost. These maps are used to plan optimal and obstacle free paths through the environment. The global path is computed before the system begins moving and takes into account all known obstacles, while the local path monitors incoming sensor data to compute suitable linear and angular velocities for the system to complete the current section of the global path. The local path is typically

computed at a rate of 20 Hz; however, this parameter is adjustable given the needs of the system.

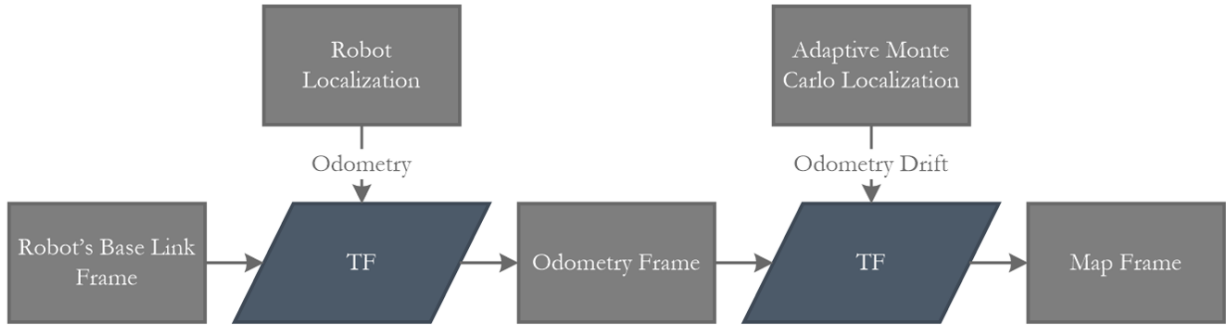


Figure 4.3: Robot Localization Framework.

4.4 Task Association and A Priori Knowledge

Once arriving in the general vicinity of the task to be accomplished, the system then locates an augmented reality (AR) tag [Siltanen], which allows it to localize and transform points of interest (POIs) associated with the AR tag into the system's frame of reference. This general localization framework is presented in Figure ??.



Figure 4.4: Initial Feature Localization Framework.

4.5 Generic Framework for Multi-Stage Computer Vision Algorithm

Insert Text Outlining the Upcoming Sections.

4.5.1 Initial Feature Location Prediction

This subsection will go through AR tags and how they are used to populate point.

4.5.2 Corrected Feature Locations

Currently the sponsor of this work uses a hole template on the object to be drilled to ensure accuracy within ± 0.3 mm. Using the predicted hole locations, given by the AR tag, an inverse kinematic solver is used to move the manipulator to the specified Cartesian location. A camera mounted on the manipulator is then used to further correct the position of the end-effector. Canny Edge Detection, Hough Transforms, as well as the camera's intrinsic characteristics and a priori knowledge of each hole's size is used to output an adjusted Cartesian location of the circle on the templet closest to the predicted position [Alter1992]. If a hole to be drilled is not found or is outside the range of the manipulator, that hole will be added to a list and the customer notified of all such holes after the operation is completed. In addition to the high precision achieved by the above technique, it can also provide a video log of all work done for inspection.

Insert Text Regarding Computer Vision Detection and Tracking System.

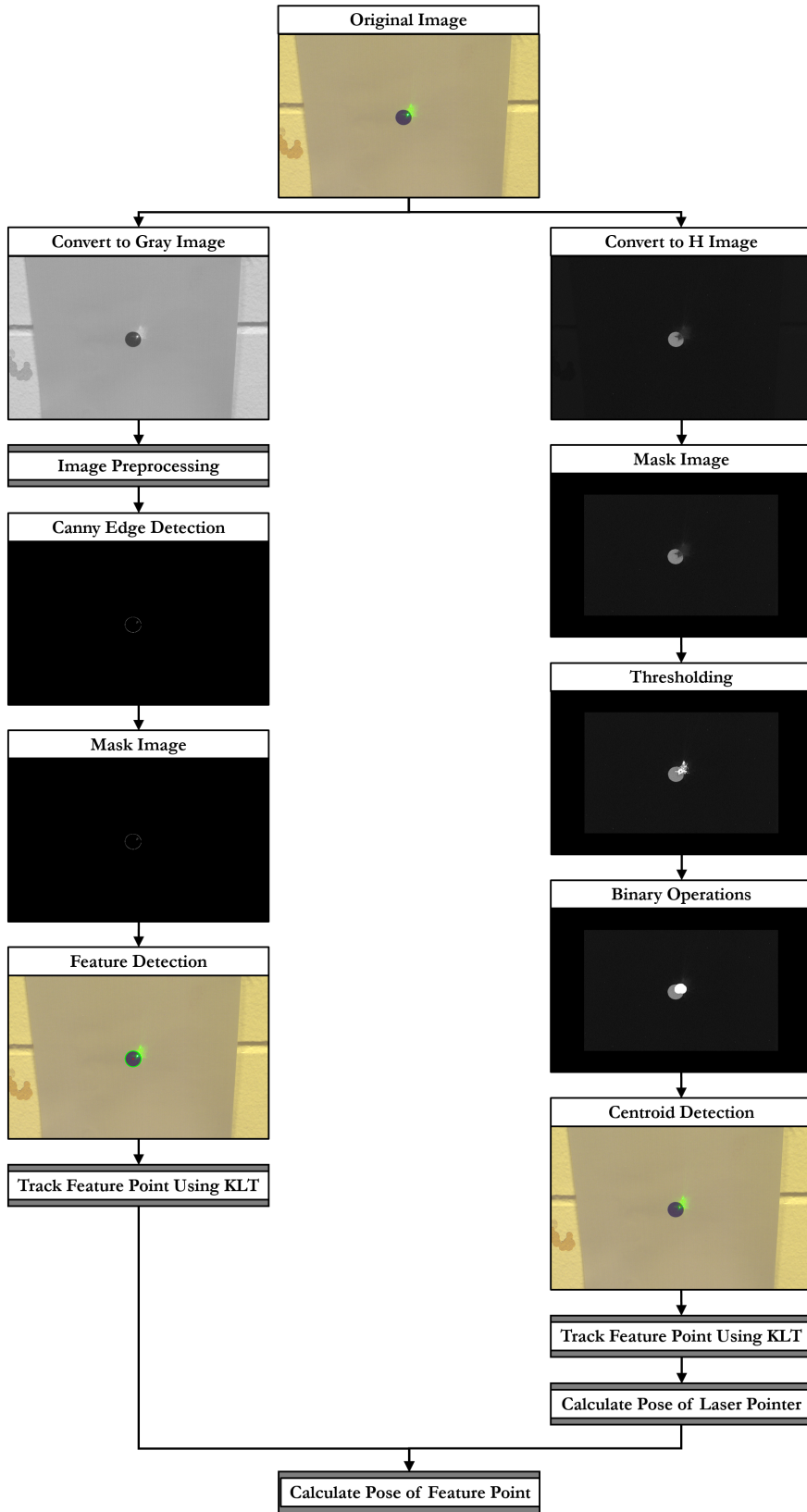


Figure 4.5: Feature Detection and Tracking Pipeline.

Insert Text Regarding Control Loop.

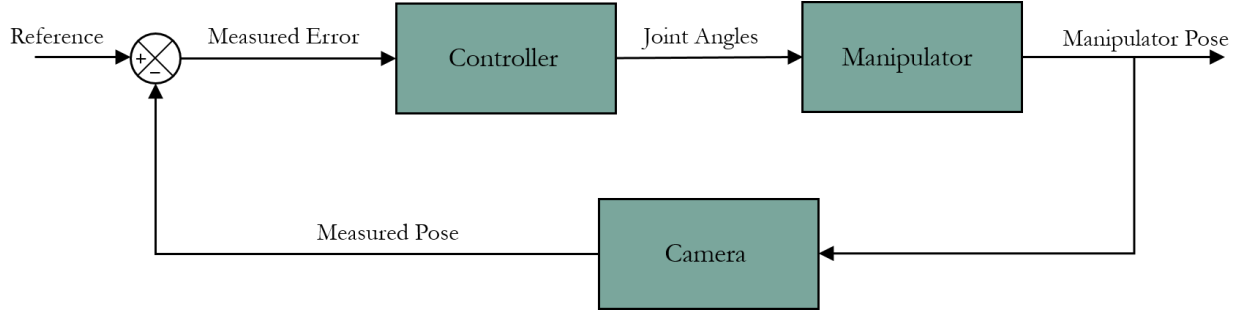


Figure 4.6: Manipulator Correction Control Loop.

4.6 Approach Implementation

Outline the upcoming sections.

4.6.1 System Overview

The generic framework of the system is depicted in Figure ???. The system allows the user to input predefined tasks. Given a priori knowledge of each tasks and their global start locations, the mobile system navigates to and performs the requested operation(s) while monitoring its battery level to ensure mission completion. The framework shown was implemented using a hierarchical state machine and was written in such a way as to make it compatible with the Robot Operating System (ROS) to ensure ease of use across differing robotic platforms.

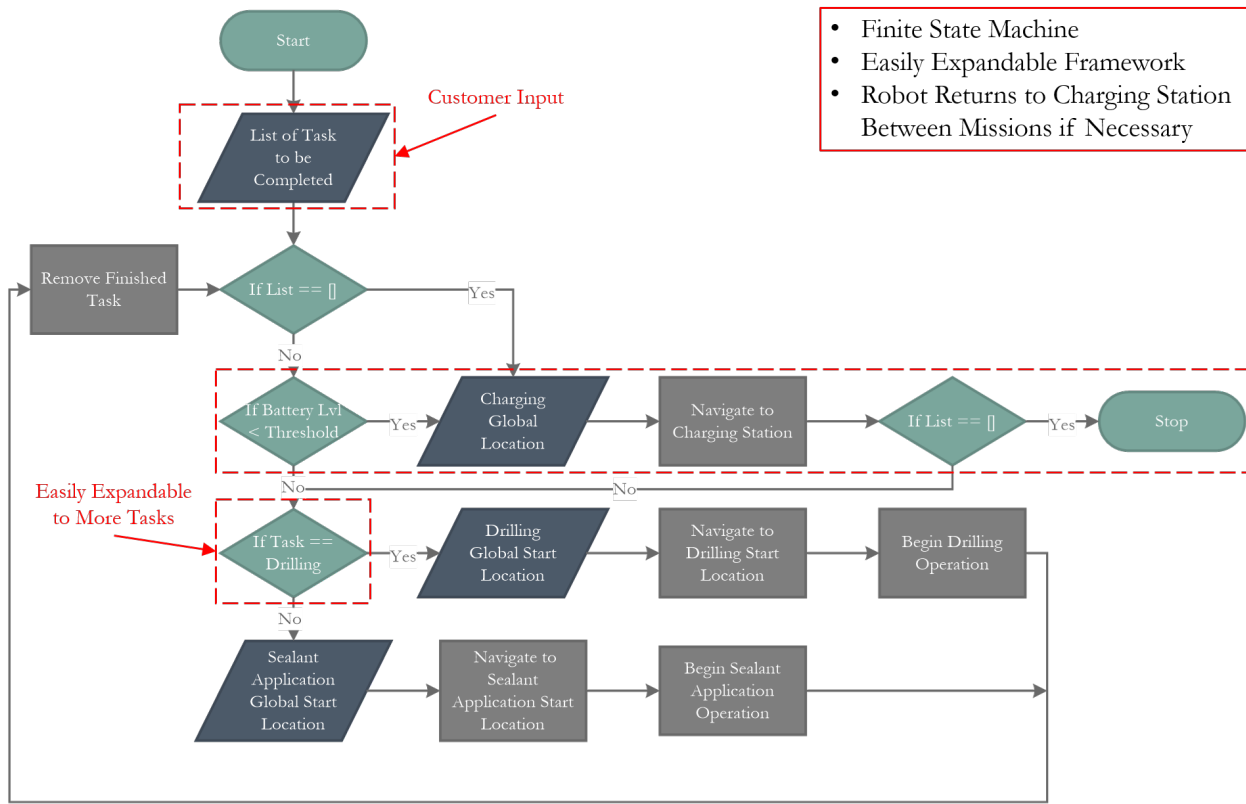


Figure 4.7: General system overview.

4.6.2 Drilling Framework

This section will go in depth into how the robot simulates drilling.

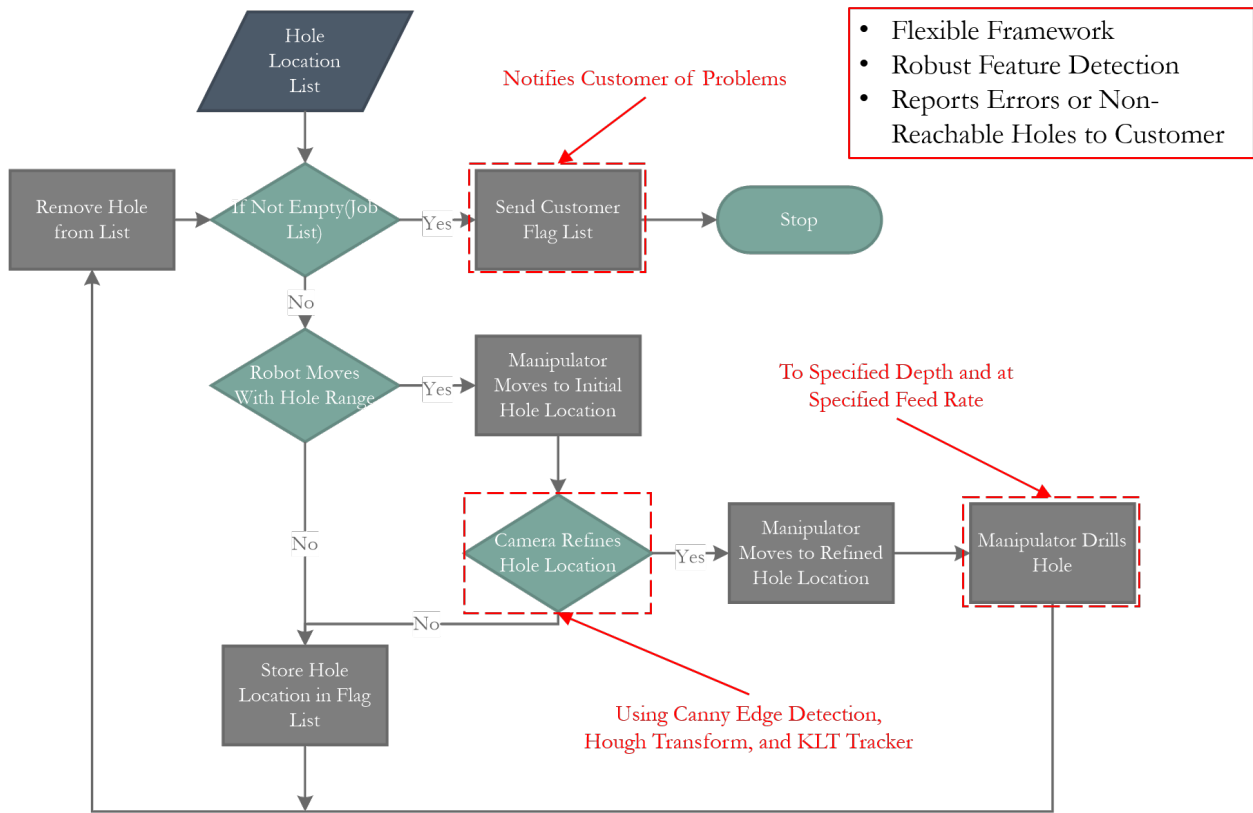


Figure 4.8: Drilling operation framework.

4.6.3 Sealant Application Framework

This section will go in depth into how the robot simulates sealant application.

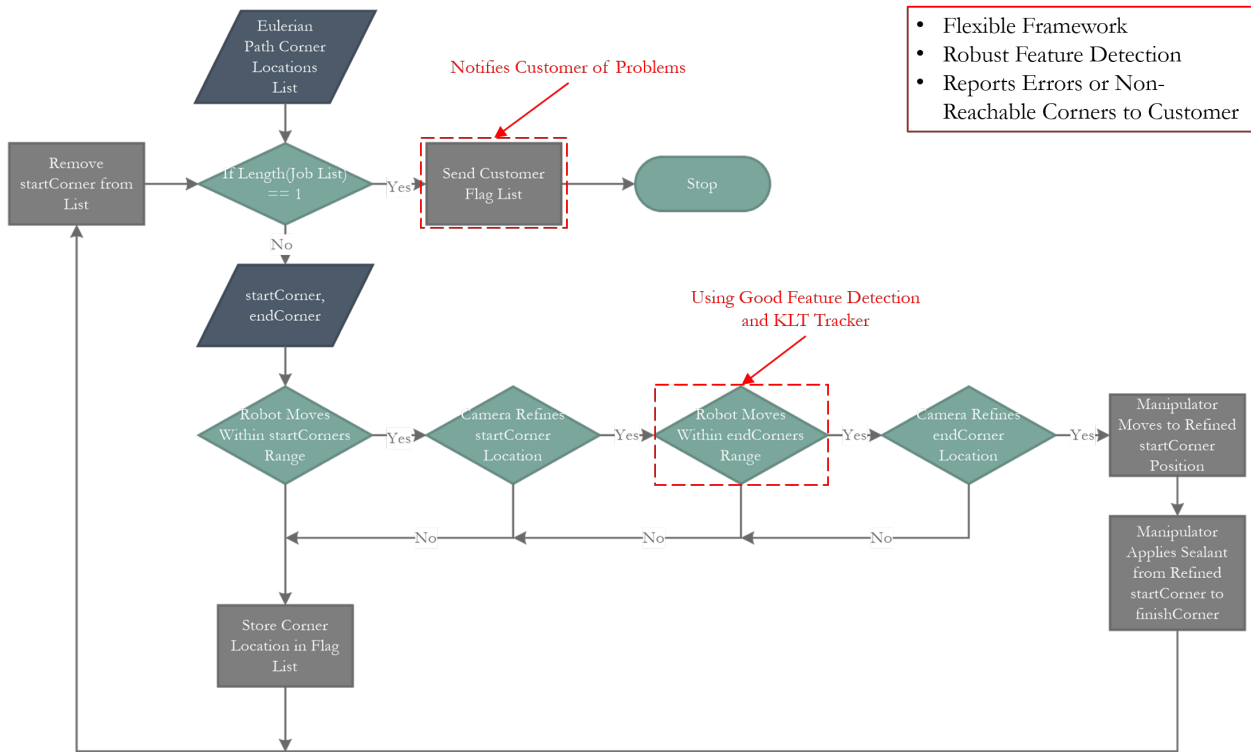


Figure 4.9: Sealant Application Framework.

4.7 Summary

Insert Text Summarizing This Chapter and Transiting to the Next.

Chapter 5

Experiments and Results

Outline the upcoming sections.

5.1 Hardware Architecture

Insert Text Regarding Robot, Sensors, etc.

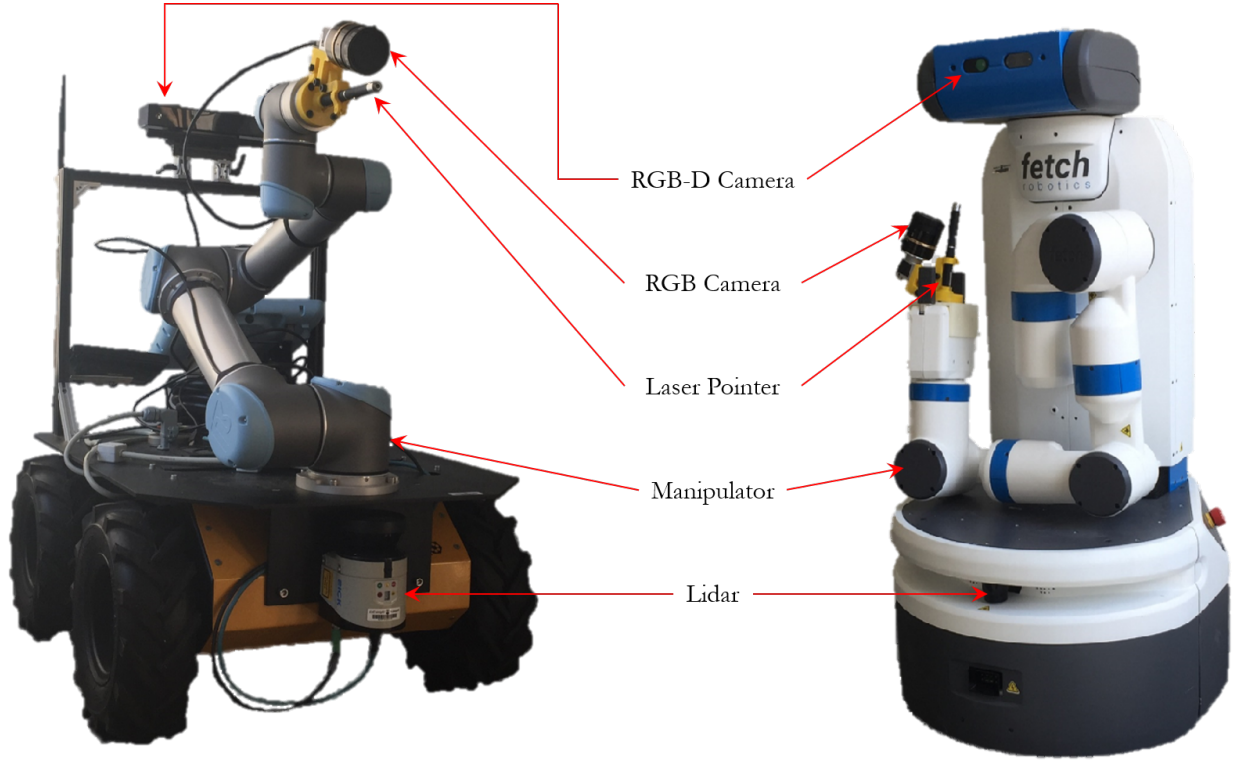


Figure 5.1: Clearpath Robotics' Husky and Fetch Robotics' Fetch Mobile Manipulator

5.2 Software Architecture

Insert Text Regarding The Software Architecture.

5.3 Experiments

Insert Text Regarding Upcoming Sections.

5.3.1 Camera Calibration Setup

Insert text setup for camera calibration.



Figure 5.2: Camera Calibration Setup.

Insert text regarding methods used for camera calibration (citing paper)

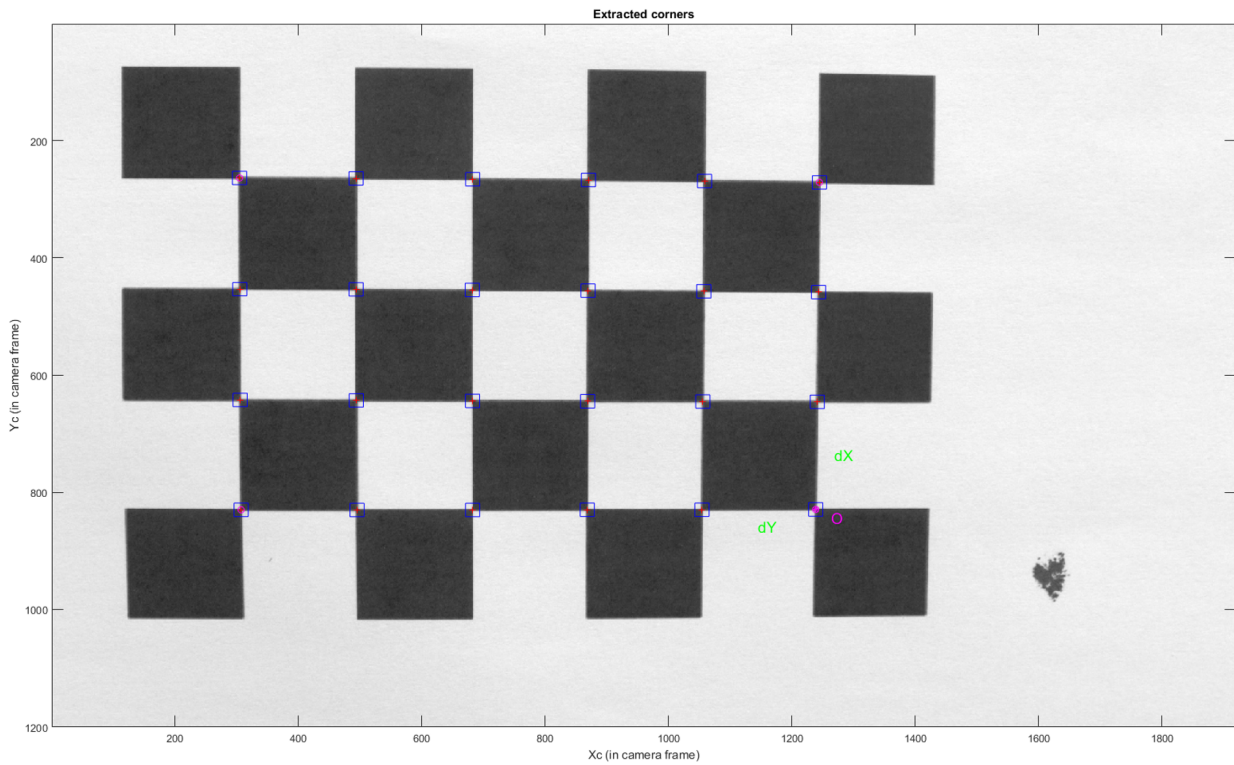


Figure 5.3: Extracted Corners of Calibration Pattern.

Insert Text and Math Regarding Calibration of Laser.

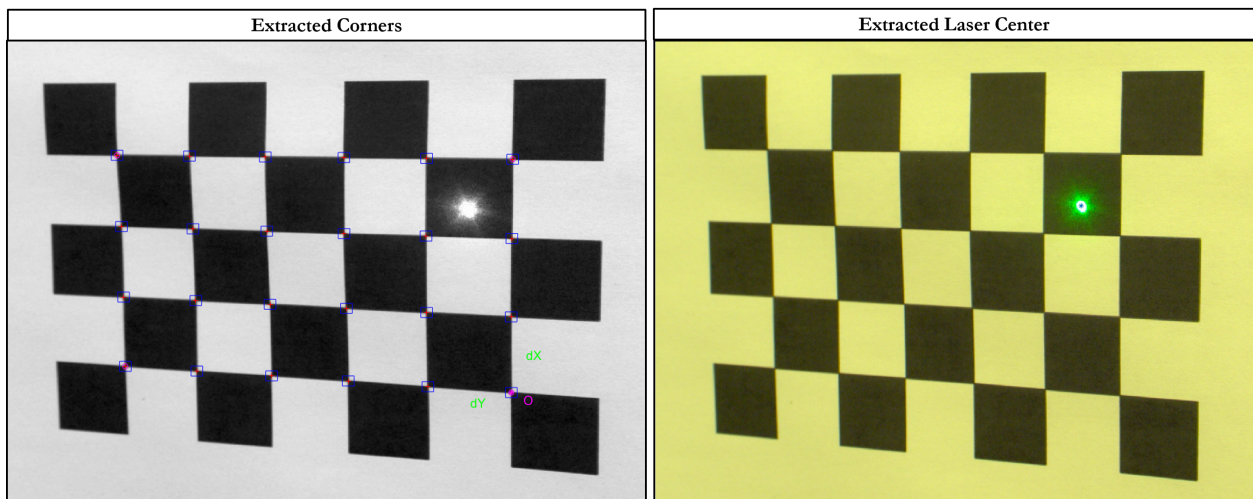


Figure 5.4: Extracted Corners and Laser Center

5.3.2 Navigation System Experimental Setup

Insert Text Regarding the Navigation System Experimental Setup.

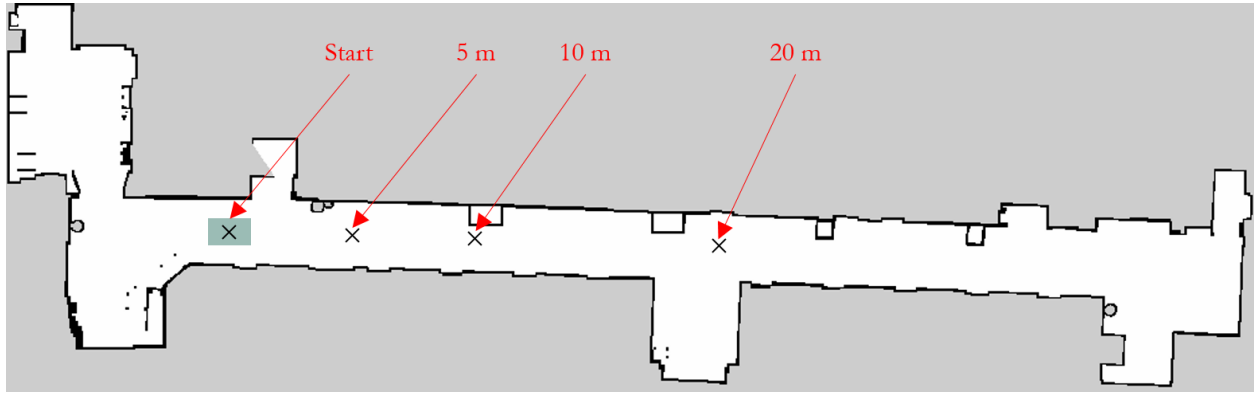


Figure 5.5: Navigation System Experimental Setup.

5.3.3 Drilling Operation Experimental Setup

Insert Text Regarding the Drilling Operations Experimental Setup.

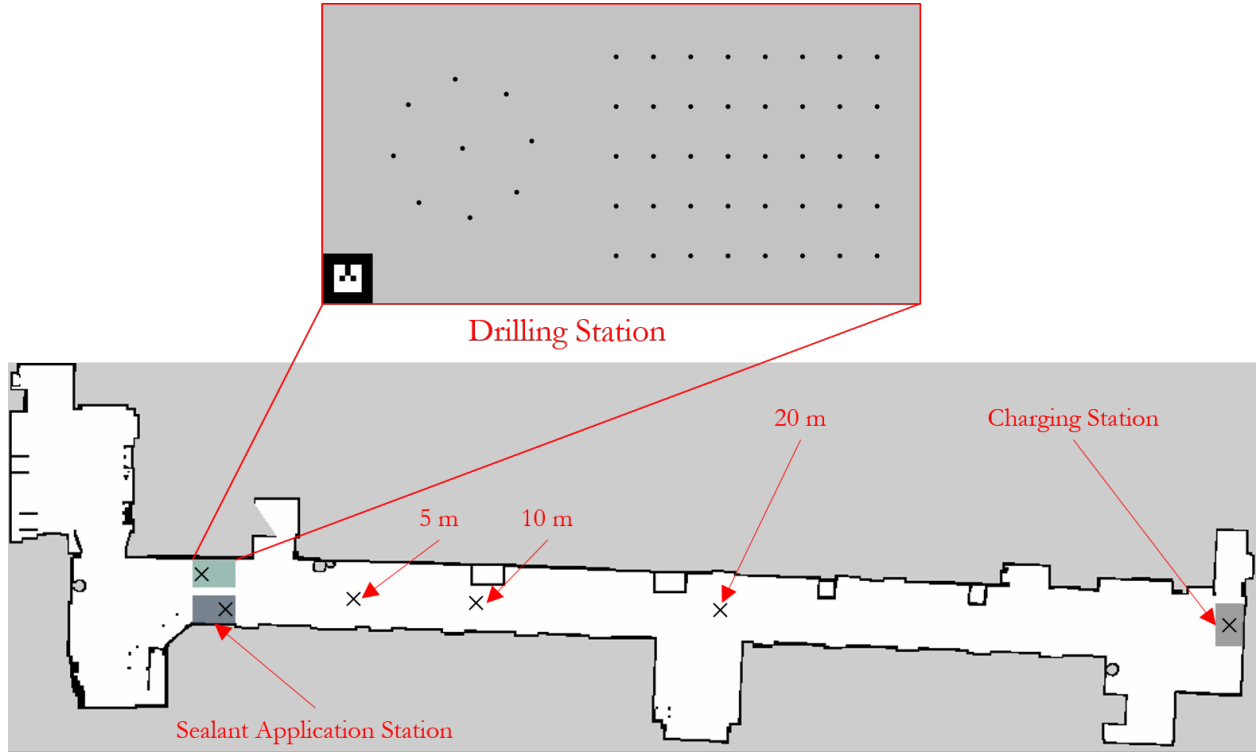


Figure 5.6: Drilling Operations Experimental Setup.

5.3.4 Sealant Application Experimental Setup

Insert Text Regarding the Sealant Application Experimental Setup.

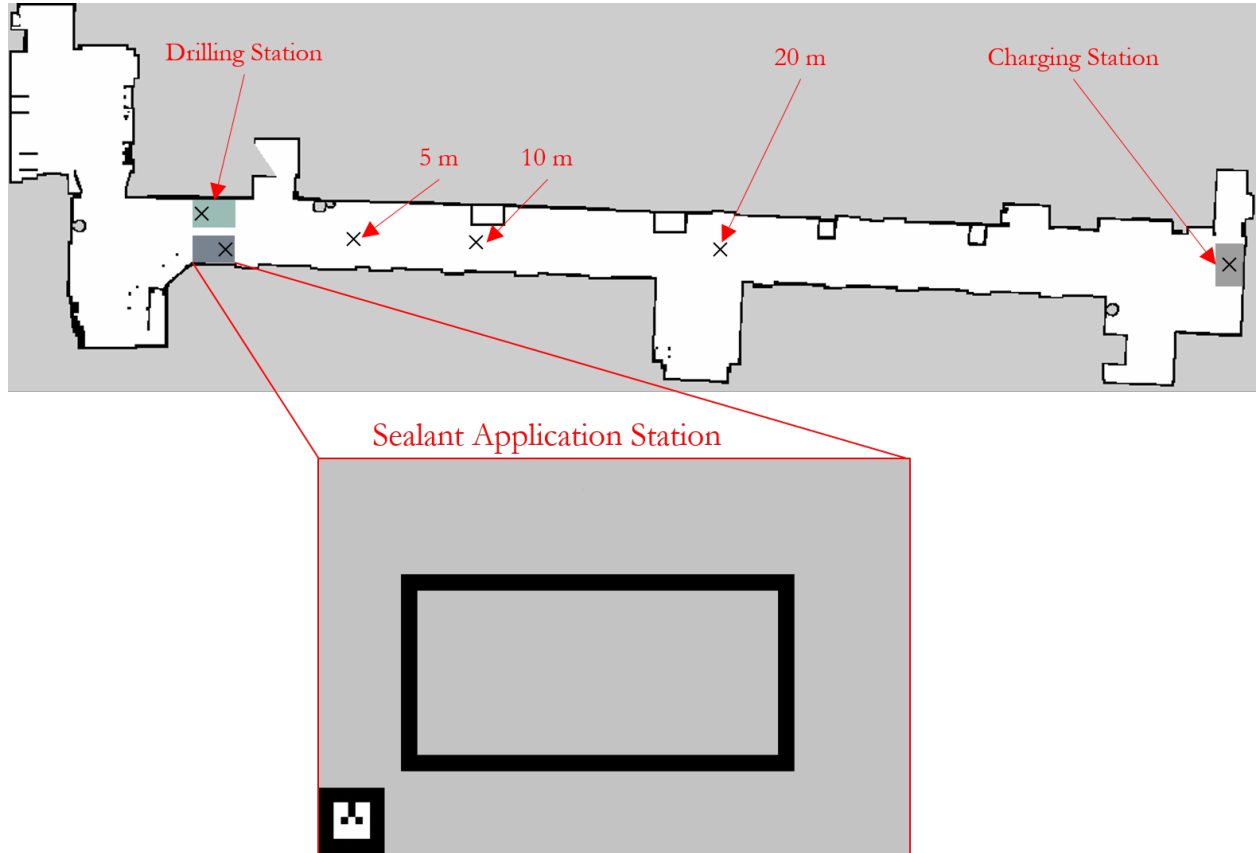


Figure 5.7: Sealant Application Experimental Setup.

5.4 Results

5.4.1 Camera Calibration Accuracy Achieved

Insert Text Regarding Pixel Error of Kinect V2.

Insert Text Regarding Pixel Error of Basler ACA150-UC.

Insert Text Regarding Pixel Error of Laser Calibration.

5.4.2 Navigation System Accuracy Achieved

Insert Text Regarding Accuracy of Navigation System and Ways To Improve Accuracy.

Table 5.1: Global Localization Accuracy Given Distance From Start - Clearpath Robotics' Husky.

	x (cm)	x std (cm)	y (cm)	y std (cm)	ψ (rad)	ψ std (rad)
5 m	6.29	4.20	4.50	3.58	0.03	0.02
10 m	4.16	3.16	2.88	2.97	0.03	0.03
20 m	6.35	4.55	2.37	1.89	0.02	0.01

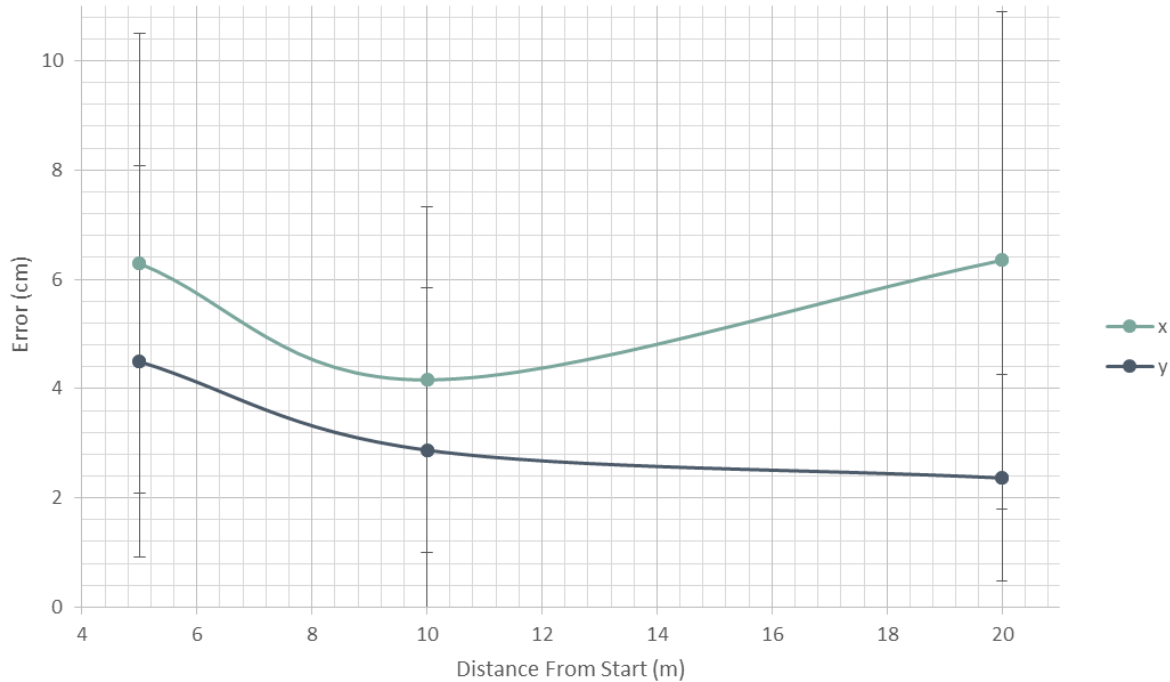


Figure 5.8: Global X and Y Localization Accuracy Given Distance From Start - Clearpath Robotics' Husky.

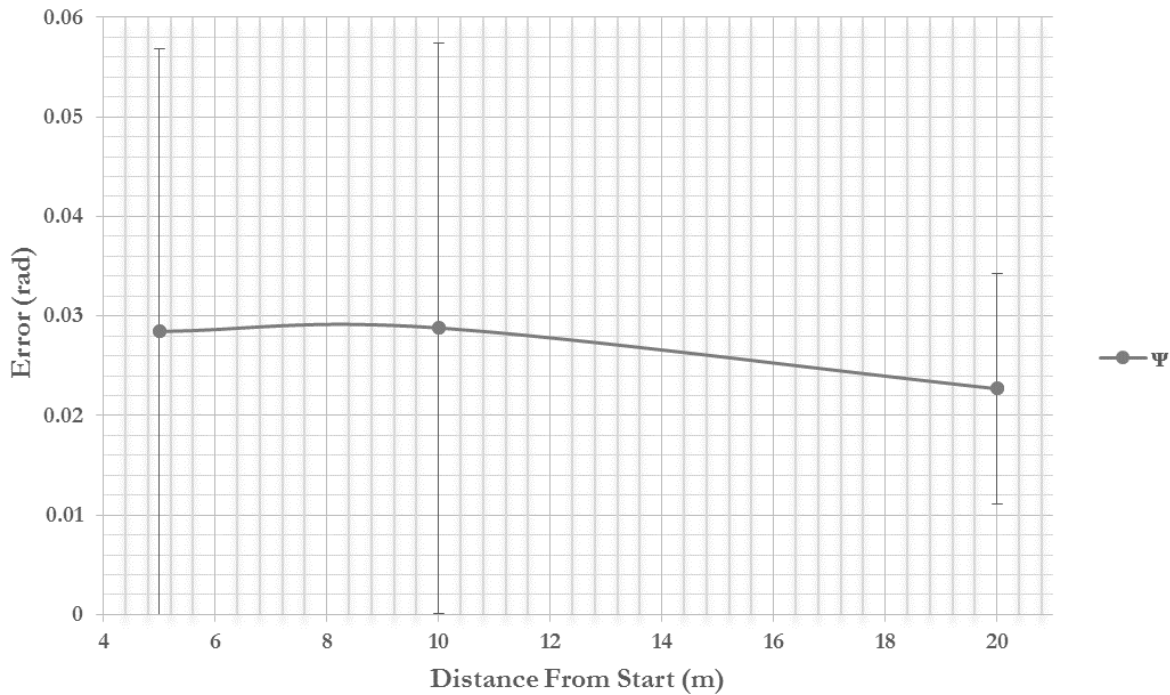


Figure 5.9: Global ψ Localization Accuracy Given Distance From Start - Clearpath Robotics' Husky.

Table 5.2: Global Localization Accuracy Given Distance From Start - Fetch Robotics' Fetch.

	x (cm)	x std (cm)	y (cm)	y std (cm)	ψ (rad)	ψ std (rad)
5 m	4.25	2.50	1.48	1.23	0.03	0.02
10 m	3.93	2.62	2.57	1.66	0.03	0.02
20 m	5.82	3.43	1.52	1.11	0.03	0.02

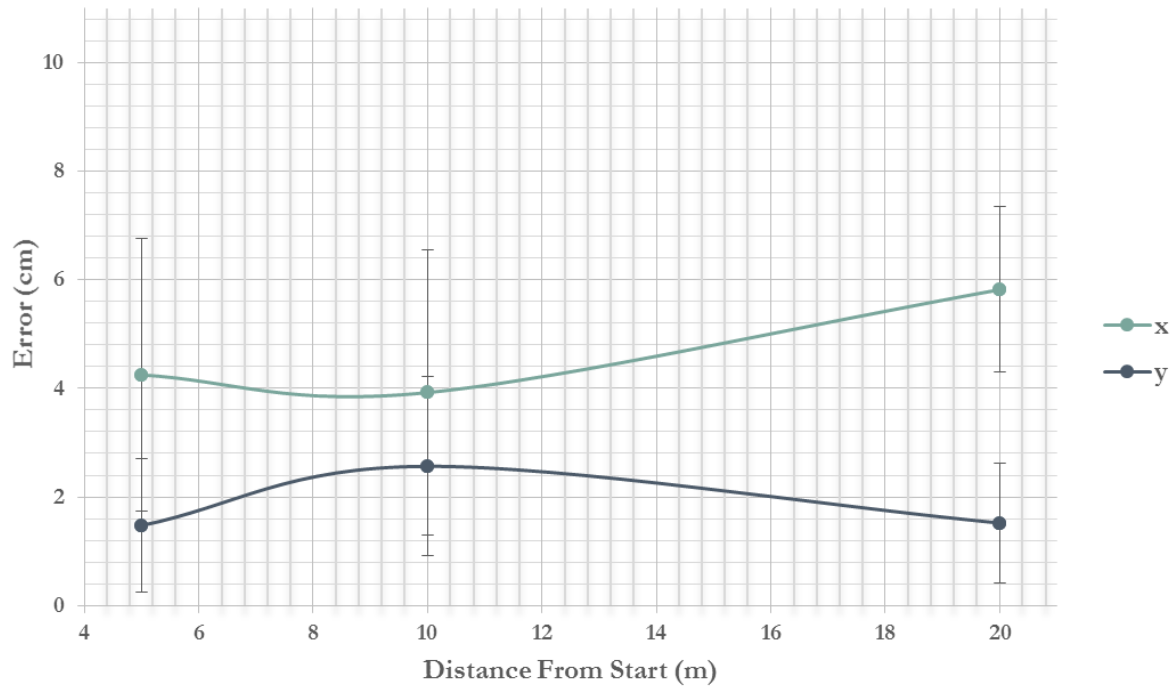


Figure 5.10: Global X and Y Localization Accuracy Given Distance From Start - Fetch Robotics' Fetch.

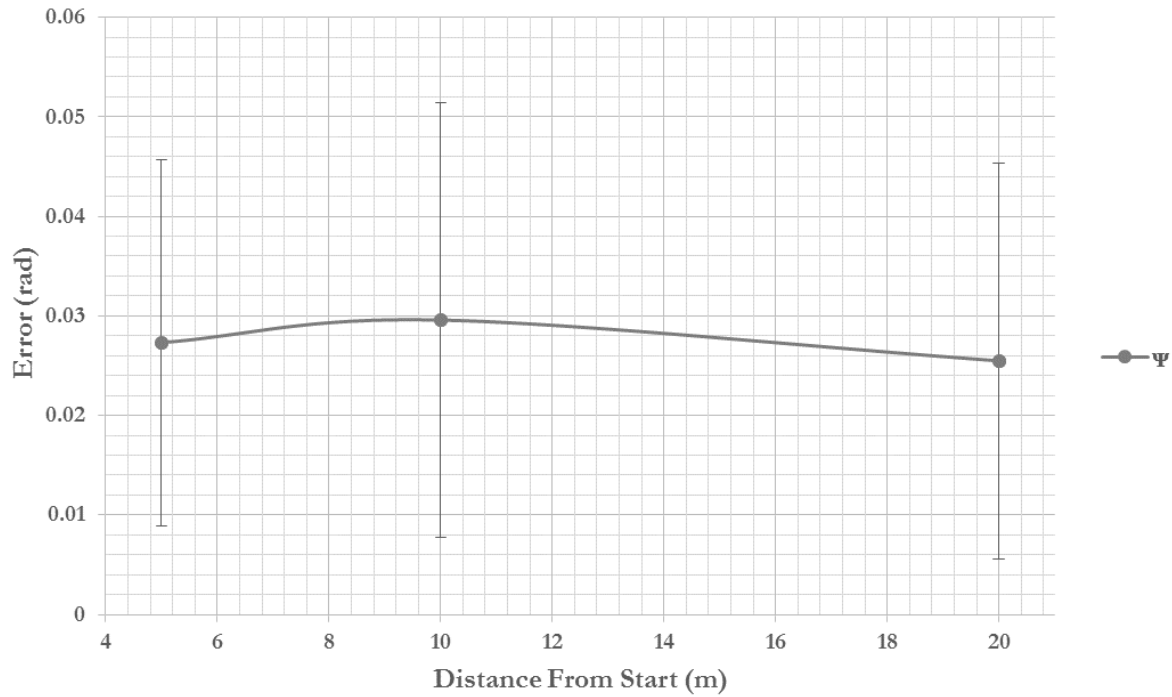


Figure 5.11: Global ψ Localization Accuracy Given Distance From Start - Fetch Robotics' Fetch.

5.4.3 Augmented Reality Tag Accuracy Achieved

Table 5.3: Augmented Reality Accuracy Given Specific Start Conditions - Primesense Carmine 1.09.

	x	x std (mm)	y	y std (mm)	z	z std (mm)
1	50.41	22.81	148.87	12.33	150.96	12.61
2	23.71	16.06	151.82	6.86	117.57	12.81
3	23.06	14.85	128.39	11.48	173.24	23.24
4	37.19	14.85	183.21	7.30	115.85	16.27
5	24.36	17.47	138.66	6.77	42.80	16.37
6	39.16	23.52	7.27	3.70	105.24	9.16

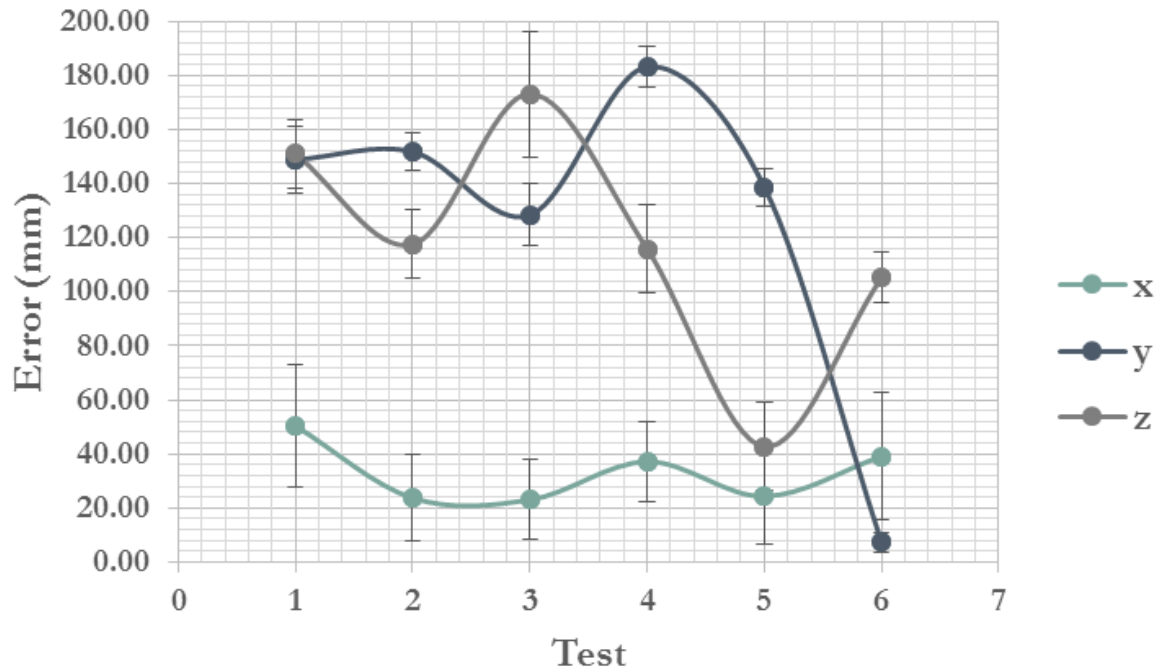


Figure 5.12: Augmented Reality Accuracy Given Specific Start Conditions - Primesense Carmine 1.09.

Table 5.4: Augmented Reality Accuracy Given Specific Start Conditions - Microsoft Kinect V2.

	x (mm)	x std (mm)	y (mm)	y std (mm)	z (mm)	z std (mm)
Test 1	14.32	9.75	4.04	1.65	84.77	2.50
Test 2	163.85	57.58	36.32	9.65	25.31	12.46
Test 3	84.33	44.37	50.31	5.48	55.24	8.57

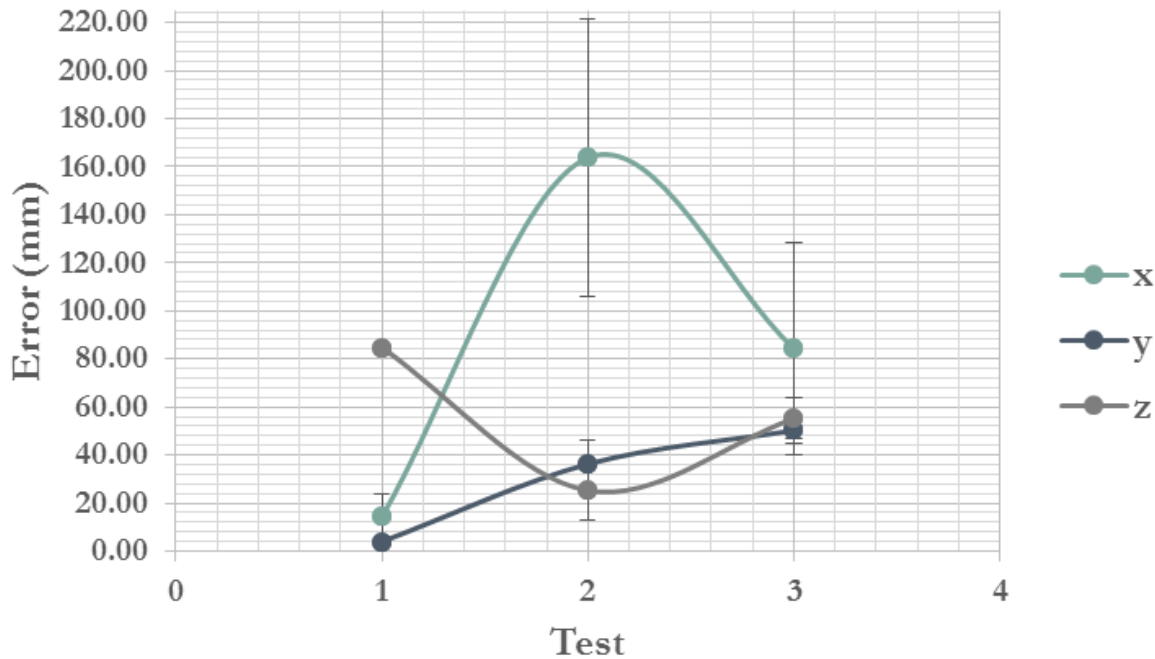


Figure 5.13: Augmented Reality Accuracy Given Specific Start Conditions - Microsoft Kinect V2.

5.4.4 Drilling Operation Accuracy Achieved

Insert Text Regarding Accuracy of Drilling Operations and Ways To Improve Accuracy.

Table 5.5: Drilling Operation Accuracy Given Distance From Work Surface.

	x (mm)	x std (mm)	y (mm)	y std (mm)	z (mm)	z std (mm)
Distance Less Than 5 mm from Hole Center	13.25	1.43	0.70	0.43	0.82	0.56
Distance Between 5 and 10 mm from Hole Center	13.62	2.71	0.66	0.39	1.89	0.46
Distance Between 10 and 20 mm from Hole Center	10.78	2.55	0.53	0.30	4.06	0.70
Distance Between 20 and 30 mm from Hole Center	10.55	2.48	0.31	0.21	10.25	1.38
Mean	12.05	2.55	0.55	0.38	4.25	3.75

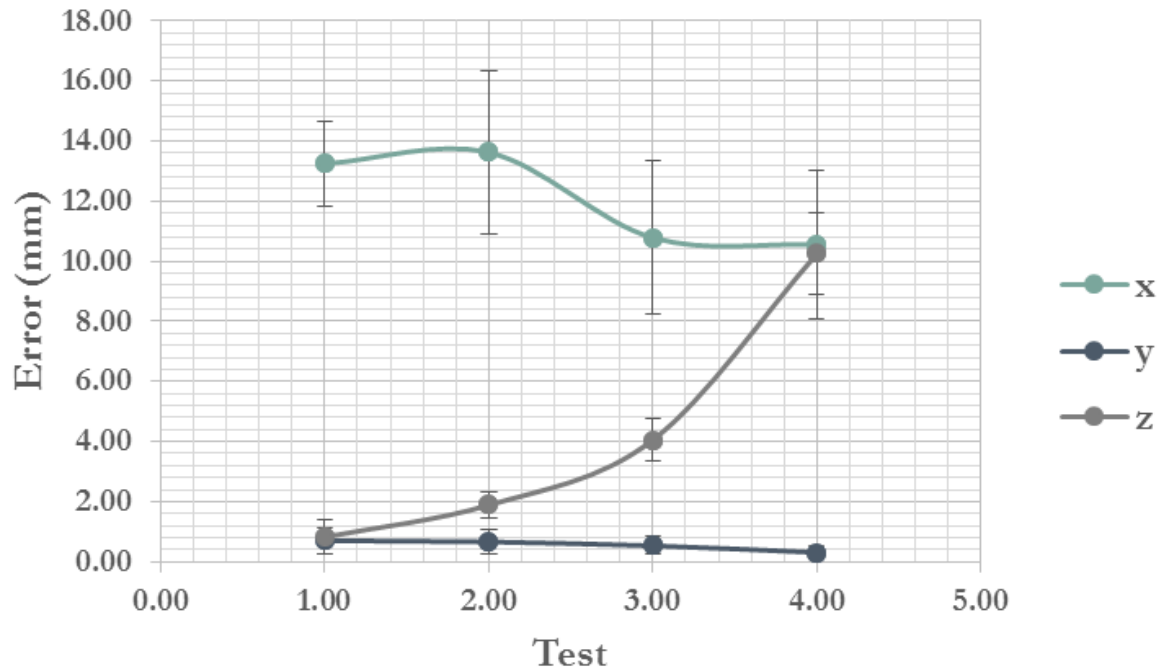


Figure 5.14: Drilling Operation Accuracy Given Distance From Feature Point.

5.4.5 Sealant Application Accuracy Achieved

Insert Text Regarding Accuracy of Sealant Application and Ways To Improve Accuracy.

Table 5.6: Sealant Application Accuracy Given Distance From Work Surface.

	x (mm)	x std (mm)	y (mm)	y std (mm)	z (mm)	z std (mm)
Distance Less Than 5 mm from Corner	10.90	2.44	1.46	0.21	1.17	0.71
Distance Between 5 and 10 mm from Corner	11.95	3.21	1.27	0.22	1.48	0.91
Distance Between 10 and 20 mm from Corner	16.32	2.56	0.78	0.34	3.81	0.32
Distance Between 20 and 30 mm from Corner	13.92	3.34	0.79	0.60	8.21	0.40
Mean	13.27	3.33	1.08	0.48	3.67	2.88

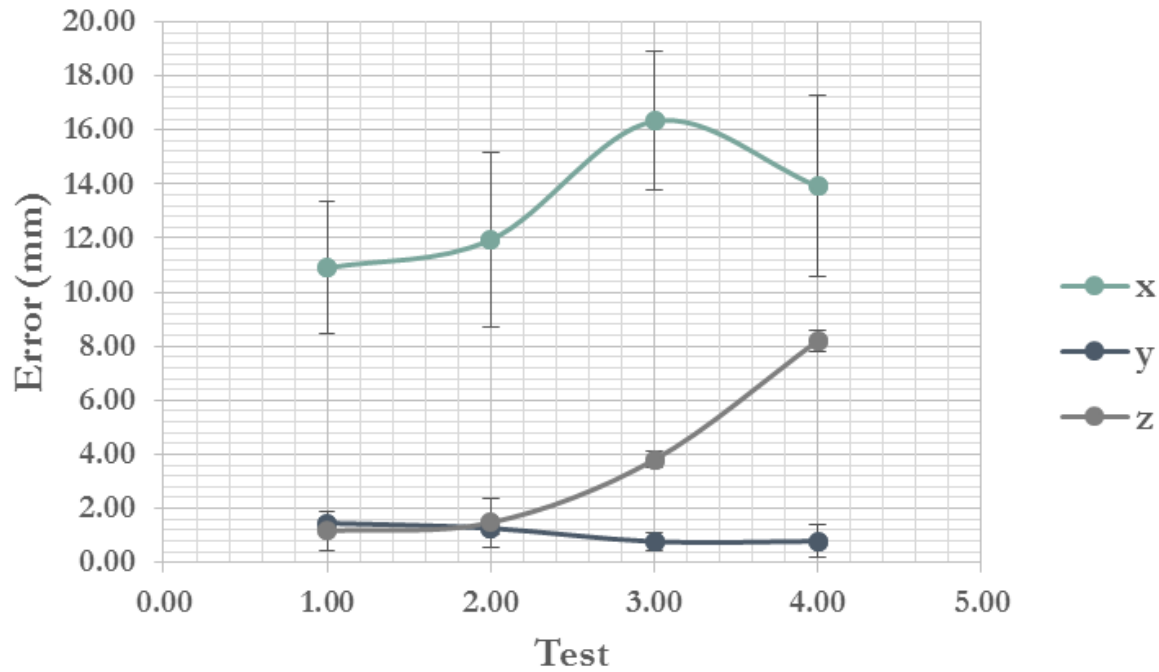


Figure 5.15: Sealant Application Accuracy Given Distance From Feature Point.

5.5 Summary

Insert Text Summarizing This Chapter and Transiting to the Next.

Chapter 6

Conclusion and Future Work

This paper showed the general framework necessary in order to solve the two main problems preventing the development and widespread adoption of ARC. These problems have caused a decrease in productivity and increase in workplace injuries/fatalities over the past several decades in comparison to other industries [Rojas2003]. These problems include the fact that typical construction sites tend to be unstructured and are continuously evolving versus the highly controlled environments found in manufacturing. Also, the relationship between the part and manipulator has been reversed, causing increased complexity not seen in manufacturing environments where the part arrives at a fixed manipulator [Feng2015]. The techniques presented allow systems to create a 2-D map of their environment, localize themselves and complete the task(s) assigned. After localizing an AR tag at the work site, the system is able to use a priori knowledge to localize POIs and complete a plethora of operations achieving an accuracy of approximately ± 2 mm based on a multifaceted computer vision approach with only a USB webcam.

Future work to be explored includes increasing the accuracy of the computer vision system to the sub-millimeter levels through the use of a machine vision camera, as well as a relatively new calibration technique developed by Feng et al [Feng2015]. In addition, automated approaches to create 3-D maps are being looked into in order to provide updated data about the robot's surroundings and task(s) automatically without human intervention. Also, human and robot collaboration over a distributed network is being explored.

Bibliography

- [1] Morgan Quigley et al. “ROS: an open-source Robot Operating System”. In: *ICRA Workshop on Open Source Software*. 2009.
- [2] *ROS.org - Powering the world’s robots*. URL: <http://www.ros.org/> (visited on 10/18/2016).
- [3] *ROS Concepts - ROS Wiki*. URL: <http://wiki.ros.org/ROS/Concepts> (visited on 10/18/2016).
- [4] James David Burton. “Development and Characterization of an Interprocess Communications Interface and Controller for Bipedal Robots”. PhD thesis. 2015.
- [5] Alonzo Kelly. *Mobile Robotics: Mathematics, Models, and Methods*. New York, NY, USA: Cambridge University Press, 2013.
- [6] *TF - ROS Wiki*. URL: <http://wiki.ros.org/tf> (visited on 10/19/2016).
- [7] *TF2 - ROS Wiki*. URL: <http://wiki.ros.org/tf2> (visited on 10/19/2016).
- [8] *URDF - ROS Wiki*. URL: <http://wiki.ros.org/urdf> (visited on 10/19/2016).
- [9] *OpenSLAM - What is SLAM?* URL: <http://openslam.org/> (visited on 10/28/2016).
- [10] J J Leonard and H F Durrant-Whyte. “Simultaneous map building and localization for an autonomous mobile robot”. In: *Intelligent Robots and Systems ’91. ’Intelligence for Mechanical Systems, Proceedings IROS ’91. IEEE/RSJ International Workshop on*. 91. 1991, 1442–1447 vol.3.
- [11] Randall C Smith and Peter Cheeseman. “On the Representation and Estimation of Spatial Uncertainty”. In: *The International Journal of Robotics Research* 5.4 (1986), pp. 56–68.
- [12] R. Smith, M. Self, and P. Cheeseman. “Estimating Uncertain Spatial Relationships in Robotics”. In: *Autonomous Robot Vehicles* 4.April (1990), pp. 167–193.
- [13] Giorgio Grisetti et al. “A tutorial on graph-based SLAM”. In: *IEEE Intelligent Transportation Systems Magazine* 2.4 (2010), pp. 31–43.
- [14] Doaa M. a Latif et al. “Comparison of Optimization Techniques for 3D Graph-based”. In: *Proceedings of the 4th European Conference of Computer Science (ECCS ’13) Recent Advances in Information Science*. October. 2013, p. 288.

- [15] Kurt Konolige et al. “Efficient sparse pose adjustment for 2D mapping”. In: *IEEE/RSJ 2010 International Conference on Intelligent Robots and Systems, IROS 2010 - Conference Proceedings*. 2010, pp. 22–29.
- [16] *HectorSLAM - ROS Wiki*. URL: http://wiki.ros.org/hector%7B%5C_%7Dslam (visited on 10/28/2016).
- [17] Stefan Kohlbrecher et al. “A flexible and scalable SLAM system with full 3D motion estimation”. In: *9th IEEE International Symposium on Safety, Security, and Rescue Robotics, SSRR 2011*. 2011, pp. 155–160.
- [18] *CoreSLAM - ROS Wiki*. URL: <http://wiki.ros.org/coreslam> (visited on 10/28/2016).
- [19] *GMapping - ROS Wiki*. URL: <http://wiki.ros.org/gmapping?distro=kinetic> (visited on 10/28/2016).
- [20] Bruno Steux and Oussama El Hamzaoui. “tinySLAM: A SLAM algorithm in less than 200 lines C-language program”. In: *11th International Conference on Control, Automation, Robotics and Vision, ICARCV 2010*. December. 2010, pp. 1975–1979.
- [21] Giorgio Grisetti, Cyrill Stachniss, and Wolfram Burgard. “Improved techniques for grid mapping with Rao-Blackwellized particle filters”. In: *IEEE Transactions on Robotics* 23.1 (2007), pp. 34–46.
- [22] *KartoSLAM - ROS Wiki*. URL: http://wiki.ros.org/slam%7B%5C_%7Dkarto?distro=groovy (visited on 10/28/2016).
- [23] *LagoSLAM - ROS Wiki*. URL: <https://github.com/rrg-polito/rrg-polito-ros-pkg> (visited on 10/28/2016).
- [24] Regis Vincent, Benson Limketkai, and Michael Eriksen. “Comparison of indoor robot localization techniques in the absence of GPS”. In: *SPIE 7664, Detection and Sensing of Mines, Explosive Objects, and Obscured Targets XV*. Ed. by Russell S. Harmon, John H. Holloway, Jr., and J. Thomas Broach. International Society for Optics and Photonics, Apr. 2010, 76641Z.
- [25] Luca Carlone and Rosario Aragues. “A linear approximation for graph-based simultaneous localization and mapping”. In: *Int. Conf. Robotics: Science and Systems*. 2011, p. 8.
- [26] João Machado Santos, David Portugal, and Rui P Rocha. “An Evaluation of 2D SLAM Techniques Available in Robot Operating System”. In: *2013 IEEE International Symposium on Safety, Security, and Rescue Robotics (SSRR)*. 2013.
- [27] *Navigation - ROS Wiki*. URL: <http://wiki.ros.org/navigation> (visited on 10/18/2016).
- [28] Sebastian Thrun, Wolfram Burgard, and Dieter Fox. *Probabilistic Robotics (Intelligent Robotics and Autonomous Agents)*. The MIT Press, 2005.

- [29] Brian P Gerkey and Kurt Konolige. “Planning and Control in Unstructured Terrain”. In: *ICRA Workshop on Path Planning on Costmaps*. 2008.
- [30] *Base Local Planner - ROS Wiki*. URL: http://wiki.ros.org/base%7B%5C_%7Dlocal%7B%5C_%7Dplanner (visited on 10/17/2016).
- [31] Richard Szeliski. *Computer Vision: Algorithms and Applications*. 1st. New York, NY, USA: Springer-Verlag New York, Inc., 2010. ISBN: 1848829345, 9781848829343.
- [32] *RGB Color Space - Wikipedia*. URL: https://en.wikipedia.org/wiki/RGB%7B%5C_%7Dcolor%7B%5C_%7Dspace (visited on 10/30/2016).
- [33] *RGB Color Model - Wikipedia*. URL: https://en.wikipedia.org/wiki/RGB%7B%5C_%7Dcolor%7B%5C_%7Dmodel (visited on 10/30/2016).
- [34] *HSL and HSV - Wikipedia*. URL: https://en.wikipedia.org/wiki/HSL%7B%5C_%7Dand%7B%5C_%7DHHSV (visited on 10/30/2016).
- [35] Alvy Ray Smith. “Color gamut transform pairs”. In: *ACM SIGGRAPH Computer Graphics* 12.3 (1978), pp. 12–19. ISSN: 00978930. DOI: 10.1145/965139.807361.
- [36] Edwin Olson. “AprilTag: A robust and flexible visual fiducial system”. In: *Proceedings of the IEEE International Conference on Robotics and Automation (ICRA)*. 2011, pp. 3400–3407. URL: <http://april.eecs.umich.edu>.
- [37] Sanni Siltanen. “Theory and applications of marker-based augmented reality”. PhD thesis. 2012.
- [38] *ARToolKit Website*. URL: <http://www.hitl.washington.edu/artoolkit/> (visited on 10/29/2016).
- [39] *ALVAR Toolkit Website*. URL: <http://virtual.vtt.fi/virtual/proj2/multimedia/alvar/index.html> (visited on 10/29/2016).
- [40] *AR Track Alvar - ROS Wiki*. URL: http://wiki.ros.org/ar%7B%5C_%7Dtrack%7B%5C_%7Dalvar (visited on 10/29/2016).
- [41] Richard Hartley and Andrew Zisserman. *Multiple View Geometry in Computer Vision*. Second. Cambridge University Press, 2004. ISBN: 0521540518.